Key Points:

- North Brazil Current rings occur independently in two layers, but often interact vertically, possibly coupling the layers
- Coupling events are concentrated near a topographic choke point, whereas the distribution of splitting is scattered
- These couplings could guide South Atlantic Water eddies past this obstacle, increasing the lifetime and distance traveled by these eddies

Author Contributions:

Conceptualization: Dante C. Napolitano, Xavier Carton
Funding acquisition: Xavier Carton, Jonathan Gula
Investigation: Dante C. Napolitano, Xavier Carton, Jonathan Gula
Methodology: Dante C. Napolitano, Xavier Carton
Project administration: Xavier Carton, Jonathan Gula
Software: Dante C. Napolitano, Jonathan Gula
Supervision: Xavier Carton, Jonathan Gula
Writing – original draft: Dante C. Napolitano

Vertical Interaction Between NBC Rings and Its Implications for South Atlantic Water Export

Dante C. Napolitano[1] , **Xavier Carton[1], and Jonathan Gula[1,2]**

[1]Laboratoire d'Océanographie Physique et Spatiale (LOPS), Univ Brest, CNRS, Ifremer, IRD, IUEM, Plouzané, France, [2]Institut Universitaire de France (IUF), Paris, France

Abstract Northwestward-propagating North Brazil Current (NBC) Rings are often destroyed upon reaching the Caribbean islands, carrying South Atlantic waters into the North Atlantic gyre and connecting the two branches of the Atlantic Meridional Overturning Circulation. Recent observations of NBC rings reported surface and subsurface cores separated by strong stratification. As independent structures, the subsurface eddies often appeared below—even if not aligned with—the surface rings. Motivated by these findings, this paper investigates the occurrence and consequences of vertical coupling between surface and subsurface NBC rings by applying a simplified theoretical model to a realistic numerical simulation. Eddy tracking in this complex simulation reveals around 1,600 instantaneous observations where eddies overlap. At each observation, we assess the eddies' vertical interaction with a $2\frac{1}{2}$-layer quasi-geostrophic framework. This interaction boils down to either coupling between the layers or a vertical splitting of the system, depending on eddy strength versus background shear. The effects of coupling include long-lived eddies that can travel longer distances. These effects are particularly important for the lower layer, where differences between coupled and non-coupled eddies are striking: about 40% of eddies with coupling travel 500 km, with ~10% carrying South Atlantic Water up to the Caribbean sea. Without coupling, eddies propagate less than 150 km. During coupling, lower-layer eddies could be driven by their surface counterparts to move offshore and bypass a topographic choke point, thus leaving the NBC retroflection region. Although still speculative, this idea explains the link between coupling and the increase in both lifetime and distance traveled for these eddies.

Plain Language Summary Recent multi-platform observations of the typical North Brazil Current (NBC) rings, extending from the surface down to 400 m, reported surface and subsurface cores kept apart by strong stratification. As independent structures, the subsurface eddies often appeared below—even if not aligned with—the surface rings. Motivated by these observations, we investigate the occurrence and consequences of vertical coupling between surface and subsurface NBC rings by applying a simplified theoretical model to a realistic numerical simulation. Eddy tracking in this simulation reveals around 1,600 observations where eddies overlap. At each observation, we assess the eddies' vertical interaction, which can reveal either coupling or splitting of the system. We find that long-lived eddies, which are able to travel longer distances, appear due to coupling. The coupling effects are particularly important for the lower layer, which may carry South Atlantic Water for 1,500 km up to the Caribbean sea. During coupling, lower-layer eddies could be driven by their surface counterparts to move offshore and bypass a topographic choke point, leaving the NBC retroflection region. Although still speculative, this idea explains the link between the coupling effect and the observed increase in both lifetime and distance traveled for these eddies.

1. Introduction

Despite major advances in what we know about oceanic eddies over the past few decades, the road ahead is still decades away from a thorough understanding of these features. While fundamental issues such as the rather arbitrary definition of an eddy continue to be debated, the scientific community has reached a consensus that eddies are an important part of the climate system. According to Z. Zhang et al. (2014), the transport of mass by mesoscale [that is, $Ro = {}^{U}/_{fL} \sim \mathcal{O}(0.1)$] eddies is only comparable in magnitude to that of the thermohaline-driven circulation, a.k.a the Meridional Overturning Circulation (MOC). The role of eddies in climate includes the transport of heat and salt anomalies and water masses of distinct characteristics around the globe (e.g., Dong et al., 2014).

Writing – review & editing: Dante C. Napolitano, Xavier Carton, Jonathan Gula

In addition to surface-intensified eddies, deep, coherent vortices (usually assembled into a broad definition of submesoscale coherent vortices, SCVs; McWilliams, 1985) are likely to further increase the contribution of eddies to volume transport in the oceans. SCVs are subsurface intensified and can travel thousands of kilometers. Except if eddies merge with other eddies or break, they undergo minimal changes in their passive tracer content from their formation to their destruction regions, where the tracer uptake or release is strongest (McWilliams, 1985). These coherent structures have recently been observed worldwide with moored ADCP (Acoustic Doppler Current Profiler; e.g., X. Zhang et al., 2022), shipboard ADCP and underway CTD (Conductivity Temperature Depth; e.g., de Marez, Carton, Corréard, et al., 2020; Lazaneo et al., 2022), ocean gliders (e.g., Bosse et al., 2015; Gula et al., 2019), Argo profiles (e.g., McCoy et al., 2020), and seismic profiles (e.g., Gula et al., 2019).

Both surface-intensified eddies and SCVs are known features in the equatorial-to-tropical North Atlantic transition region, where large eddies are formed in the North Brazil Current (NBC) retroflection (e.g., Nof & Pichevin, 1996; Silveira et al., 2000) and propagate northwestward, often being destroyed as they approach the Caribbean islands (e.g., Andrade-Canto & Beron-Vera, 2022; Fratantoni & Richardson, 2006). They are called NBC rings (Johns et al., 1990; Richardson et al., 1994) and come in different varieties (e.g., Bourlès et al., 1999; Fratantoni & Glickson, 2002; Fratantoni & Richardson, 2006; Johns et al., 2003; Wilson et al., 2002). They play a major role in the cross-hemispheric transport of South Atlantic waters into the North Atlantic gyre, connecting the two branches of the Atlantic MOC (AMOC; e.g., Johns et al., 1990, 2003) in what has recently been defined as the "direct" route (Chidichimo et al., 2023; Tuchen et al., 2022). Early estimates by Johns et al. (1990) and Richardson et al. (1994) suggested that the NBC rings would transport about 3 Sv (1 Sverdrup: 10^6 m^3 s^{-1}) of South Atlantic Water (SAW) to the northwest. These include the Salinity Maximum Water (SMW), the South Atlantic Central Water (SACW), and the surface Tropical Water (TW), brought in from the South Atlantic (Stramma & Schott, 1999) and modified by the North Atlantic waters and the Amazon River inflow (Hellweger & Gordon, 2002). Years later, estimates of the total SAW transport accounted for by NBC rings were increased to 9.3 Sv, by considering the contribution of thick subsurface NBC rings in addition to the surface-intensified, satellite-tracked NBC rings (Johns et al., 2003). From three vertical sections along the Caribbean islands, Rhein et al. (2005) suggested that about $^1/_3$ of the total SAW transport (∼3 out of 9.1 Sv) could be related to these long-lived, subsurface NBC rings.

The core of the subsurface NBC rings is generally located within the 1,024.5–1,027.1 kg m^{-3} isopycnal layer, that is, the domain of the salinity maximum and central waters (e.g., Bueno et al., 2022; Kirchner et al., 2009; Rhein et al., 2005; Stevens et al., 2021, although the limits and definitions vary in the literature). This layer is of particular interest for climate regulation as it contains most of the water of South Atlantic origin (e.g., Metcalf & Stalcup, 1967) that reaches the North Atlantic MOC, with particular interest drawn to the SACW, which on average fills 80%–100% of the central layers (Kirchner et al., 2009). Understanding the SACW pathways is key to assessing climate change, as this water mass formation in the subtropical surface ocean is responsible for the uptake and redistribution of roughly 10% of the global upper ocean warming (e.g., Chidichimo et al., 2023) through ventilation of the main thermocline (e.g., Kolodziejczyk et al., 2019).

With unprecedented measurement campaigns such as the recent EUREC4A-OA project (Karstensen et al., 2020; Speich et al., 2021; Stevens et al., 2021; Subirade et al., 2023), which promoted multi-platform, high-resolution observations, attention was again drawn to the different types of NBC rings previously described in the literature. These include the typical large NBC rings extending from the surface down to over 400 m, a shallower (∼200 m) surface intensified variety, and a subsurface intensified one occupying the ∼200–400 m range (e.g., Johns et al., 2003; Wilson et al., 2002). Of the three, the former may have two distinct surface and subsurface cores (e.g., Fratantoni & Glickson, 2002; Stevens et al., 2021). Indeed, upstream of the NBC retroflection region, both surface and subsurface anticyclones have been shown to coexist independently in the NBC domain; Simoes-Sousa et al. (2021)'s Barreirinhas Eddies originate from the stacked NBC-NBUC (North Brazil Undercurrent) current system, in which both currents may have separate cores due to the high stratification that decouples the density layers. It is possible that a footprint of the original NBC-NBUC configuration crossing the Equator still drives independent cores embedded in the NBC retroflection region where NBC rings are shed.

Observations from the EUREC4A-OA campaign captured surface and subsurface eddies separated by strong stratification (Stevens et al., 2021; Subirade et al., 2023). Although considered as independent structures, the subsurface eddies often appeared below—though not aligned with—the surface rings, a picture also shown in the
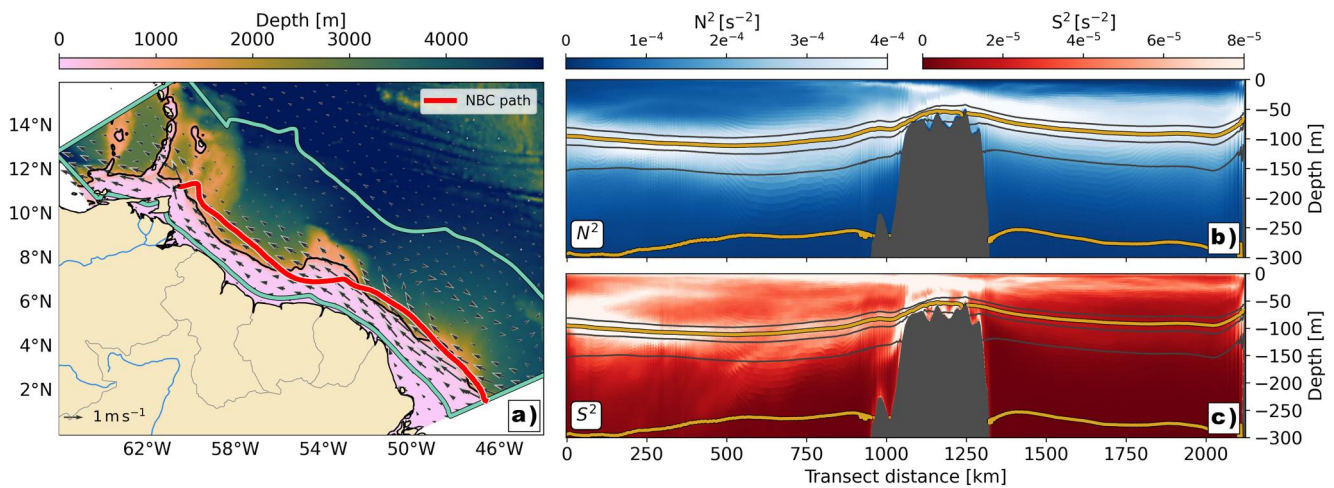
Figure 1. The GIGATL3 study region and layer definition. (a) Local bathymetry (colors) and the eddy boulevard (green highlighted area), with the NBC path (red line) closely following the NBC main axis (indicated by arrows) around 1000 m (black line). The NBC path is defined by projecting the 20-m isobath offshore onto the 1,000 m isobath. (b) 2-year mean stratification (N^2) and (c) vertical shear (S^2) along the NBC path. Gold lines mark the $\sigma_0 = 1{,}024.5$ kg m^{-3} and $\sigma_0 = 1{,}026.9$ kg m^{-3} layer boundaries. Black lines mark the 1,024, 1,025, and 1,026 kg m^{-3} isopycnals for reference.

early stages of vortex vertical interaction (e.g., Nof & Dewar, 1994). Following Polvani (1991)'s theory on the vertical alignment of eddies, Nof and Dewar (1994) showed in laboratory experiments how anticyclones occupying different layers in a stratified fluid can align vertically. Later, vertical alignment was observed in three cases for Meddies (Mediterranean Water eddies) under the Azores Current (Tychensky & Carton, 1998). Finally, Reinaud and Carton (2020) numerical experiments have extensively explored the vertical coupling under different flow configurations, leading us to question: Are the surface and subsurface NBC rings really independent structures throughout their life cycle? Or do eddies in the NBC interact vertically when they are strong enough to overcome the local vertical shear? Furthermore, could local and/or larger-scale effects of a possible coupling affect the cross-hemisphere transport of SAW?

The main objective of this study is to investigate the occurrence and consequences of vertical coupling between surface and subsurface NBC rings. To this end, we apply a simplified theoretical framework to a realistic regional numerical model. In the next section, we briefly describe the model configuration and track NBC rings through different layers. We then introduce the reader to the theory used here and how it fits our simulated eddies. Finally, we discuss the occurrence, distribution, and implications of vertical coupling between NBC rings.

2. The NBC Rings in the Numerical Simulation

We use two years of simulation with 12-hr averages to smoothly track the eddies. The simulation, called GIG-ATL3 (Gula et al., 2021), uses the model CROCO (Coastal and Regional Ocean COmmunity model, based on the Regional Oceanic Modeling System; Shchepetkin & McWilliams, 2005) over the Atlantic Ocean with a nominal 3 km horizontal resolution and 100 terrain-following vertical levels. The simulation uses SODA's (Simple Ocean Data Assimilation; J. A. Carton & Giese, 2008) initial and boundary conditions, hourly CFSR (Climate Forecast System Reanalysis; Saha et al., 2010) atmospheric forcing, a k-ϵ turbulence closure scheme (Umlauf & Burchard, 2003) for parameterization of vertical mixing, and 30-s arc bathymetry (SRTM30plus data set; Becker et al., 2009). The Amazon River input is a monthly climatology from Dai and Trenberth (2002). The simulation has no tides and is initialized in January 2004. We use the simulated years 2011 and 2012. The family of GIGATL simulations (cf. Gula et al., 2021, for the source code) were previously used for a wide range of applications (e.g., Qu et al., 2021; Ruan et al., 2021; Tagliabue et al., 2022; Vic et al., 2022).

2.1. An Overview of NBC Rings at Various Depths

A subset of the model domain is shown in Figure 1a. This subdomain extends over 20° in both south-north and east-west directions, and we conduct our analyses in the along-isobath strip highlighted in Figure 1a. The mean NBC enters the region around 2°N and flows northwestward along the 1000-m isobath (Figure 1a), up to the

Caribbean islands. To separate surface from subsurface flows, we restrict our analyses to two separate layers (Figures 1b and 1c) along this ~2,000 km strip termed the "eddy boulevard" (Stevens et al., 2021). The layers' definition follows that of the water masses they primarily transport, that is, the TW (layer 1, between the surface and $\sigma_0 = 1,024.5$ kg m^{-3}) and the SMW–SACW (layer 2, between $\sigma_0 = 1,024.5$ and $1,026.9$ kg m^{-3}). As noted above, water mass names and density limits can vary in the literature. Our definitions closely follow those used by Rhein et al. (2005) and Kirchner et al. (2009) for the TW, SMW, and upper SACW. We choose to combine the latter two into one "thermocline layer" which transports most of the SAW (Bueno et al., 2022; Kirchner et al., 2009). We also support our choice of isopycnals from the model's vertical sections of stratification ($N^2 = \frac{g}{\rho_0}\rho_z$; Figure 1b) and vertical shear ($S^2 = u_z^2 + v_z^2$; Figure 1c) along the NBC path. (In the previous definitions, subscripts denote derivatives in the indicated Cartesian direction.) Figures 1b and 1c show that the lower (upper) limit of layer 1 (2) lies in the highest N^2 and S^2 regions, suggesting a dynamical boundary between these layers.

Historically, eddies have been identified by satellite altimeters via their sea surface height (SSH) signature (see Fu et al., 2010; Morrow et al., 2019, for past and future applications of satellite altimetry to eddy dynamics). Recently, Subirade et al. (2023) tracked surface NBC rings via SSH and compared their characteristics with EUREC4A-OA *in situ* data. However, within the high-shear, stratified background flow in the NBC region, subsurface-intensified eddies may not be visible in the SSH field (e.g., Stevens et al., 2021). Therefore, we take advantage of the 3D velocity field of the numerical simulation and avoid the debate about whether deeper eddies are detected by altimetry or not. We then identify and track the eddies in each layer independently using the Okubo-Weiss parameter (OW), a relationship between rotation and deformation of the flow (Okubo, 1970; Weiss, 1991). Within the eddy boulevard (Figure 1a), we compute OW (as in Isern-Fontanet et al., 2004) for each layer k,

$$\mathrm{OW}|_{k=1,2} = s_\perp^2 + s_\parallel^2 - \zeta^2, \tag{1}$$

and average within the layers' limits. In Equation 1, $s_\perp = u_x - v_y$ and $s_\parallel = v_x + u_y$ are, respectively, the normal and shear components of the strain field, and $\zeta = v_x - u_y$ is the vertical component of the relative vorticity of layer k.

To get an overview of the propagation of intense rotating structures (henceforth treated as eddies), we average OW along the model's x-direction (approximately cross-isobath) and take its $^1/_3$ quantile, that is, the ~33% most negative values of OW. The space-time evolution of such eddies is depicted in Figure 2a. Slanted bands of $<\mathrm{OW}_1>^{1/3}$ indicate the northwestward propagation of eddies after they gain strength around 4°N (~250–500 km). Superimposed on these, bands of strong $<\mathrm{OW}_2>^{1/3}$ ($\leq -7.5 \times 10^{-11}$) indicate the motion of layer-2 eddies. Interestingly, layer-2 eddies remain quasi-standing within the NBC retroflection (between 0 and ~500 km), except for a few rogue trajectories that travel more than 1,000 km downstream of this region. Moreover, these trajectories often—if not always—propagate along strong $<\mathrm{OW}_1>^{1/3}$, as if closely followed by an accomplice eddy on layer 1.

Specific examples are plotted to show the presence of the NBC rings in layer 1 (Figures 2b–2d) and in layer 2 (Figures 2e–2g). Numerous SCVs are also visible in both layers. In the tropical ocean, submesoscales [$Ro \sim \mathcal{O}(1)$] (and SCVs therein) can be up to one order of magnitude bigger than those in classical mid-latitude examples, reaching up to 50–200 km (e.g., Marchesiello et al., 2011). Although some of these smaller structures tend to be cast aside in the next sections due to the nature of our QG analysis, they deserve future attention as they have been recently suggested to be double agents in the route to energy dissipation, acting as conveyors of energy (and tracers) to larger scales via the inverse cascade (e.g., Z. Zhang et al., 2023) or cascading energy down to smaller scales (e.g., Lazaneo et al., 2022). Considering the larger structures yielding a strong $<\mathrm{OW}_k>^{1/3}$, three possible settings (also depicted from schematics in Bourlès et al., 1999) are drawn from Figure 2a: (a) on 22 Aug 2011, an eddy exists in layer 1, marked by strong $\mathrm{OW}_1 < 0$, but no eddy is observed in layer 2 (Figures 2b and 2e); (b) conversely, OW_2 on 16 Apr 2011 marks a layer-2 eddy within the NBC retroflection, but the signal is absent in layer 1 (Figures 2c and 2f); (c) on 11 Sep 2012, the superimposed OW signals show concomitant eddies in both layers (Figures 2d and 2g).

The vertical sections of the eddies depicted in Figures 2b–2g reveal the different types of eddies in the region (Figure 3), as previously observed by Fratantoni and Richardson (2006). The surface eddy on 22 Aug 2011
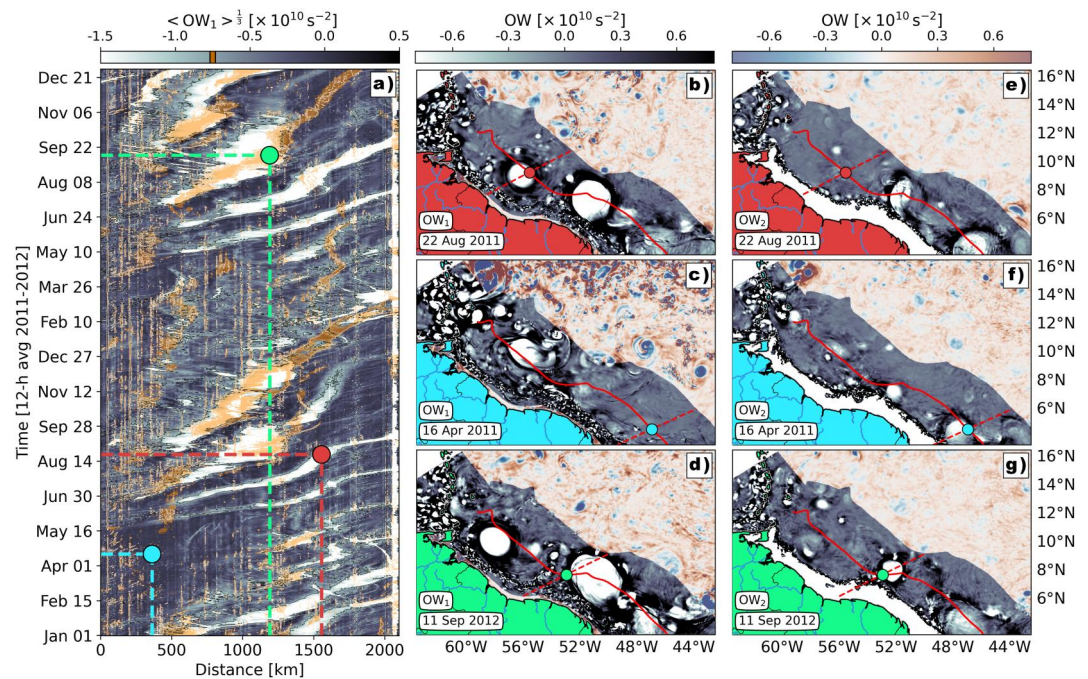
Figure 2. (a) Hovmöller diagram of $\langle OW_1 \rangle^{1/3}$ ($\langle \rangle$ denotes spatial average on the model x-direction and $1/3$ denotes a 0.33 quantile). Orange bands show $\langle OW_2 \rangle^{1/3}$ values stronger than an arbitrary threshold -7.5×10^{-11}. Circles indicate color-coded features displayed in the right panels via snapshots of selected OW_1 (b–d) and OW_2 (e–g). Daily OW (colors) highlights the presence or absence of eddies in the eddy boulevard (grayscale) of each layer. The red solid line is the Hovmöller path and the red dashed line is the direction of "zonal" averaging in the curvilinear grid.

presents a coherent core entirely within layer 1 (Figure 3a), displaying velocities $>|0.5|\text{m s}^{-1}$ from the surface to 100 m (Figure 3d) and the deepening of the 1,024.5 kg m^{-3} isopycnal at its center. This isopycnal coincides with a local maximum of stratification (Figure 3g), separating shallow surface NBC rings from subsurface ones (Stevens et al., 2021). The example on 16 Apr 2011 shows indeed a subsurface NBC ring separated by strong stratification from the upper layer, where eddy activity is much weaker (Figure 3b). The $>|0.5|\text{m s}^{-1}$ core is entirely within layer 2, below extreme N^2 values of up to 1×10^{-3} (Figures 3e and 3h). When eddies overlap, as on 11 Sep 2012, the 1,024.5 kg m^{-3} isopycnal still confines a strong NBC ring within layer 1 ($>|1.5|\text{m s}^{-1}$), while a smaller subsurface NBC ring occupies layer 2 (Figures 3c and 3f) demonstrating the independent nature of these eddies (Figure 3i). It is important to note that the lower boundary of layer 2 is chosen primarily to represent a layer with a high percentage of SACW, rather than a layer that is dynamically independent of the layers below it (for precise definition of eddy boundaries, the use of potential vorticity anomaly is advised, cf. Morel et al., 2023, see examples for NBC rings in Subirade et al., 2023). As shown in Figures 3c and 3f (and partially in Figures 3b and 3e; see also Fratantoni & Richardson, 2006), subsurface eddies can extend into deeper layers. In some cases, the system may also exhibit a near-barotropic configuration, blurring the boundary between the structures. Such observations are treated as special cases. Nevertheless, the consideration of initially independent structures should not affect the main results, as will be discussed later.

Looking at the horizontal and vertical structure of the NBC rings and their propagation, the question naturally arises. Do layer-2 eddies randomly follow layer-1 eddies? Or is there a mechanism at work that couples these eddies by vertical interaction when they occasionally overlap (Figure 3c)?

We address the question above by applying a theoretical eddy-interaction model to the realistic numerical simulation. But first, we need to identify and track the NBC rings in GIGATL3.

2.2. Zoology of the NBC Rings

We identify and track eddies in the simulation using the *py-eddy-tracker* algorithm (Mason et al., 2014; Pegliasco et al., 2022, https://py-eddy-tracker.readthedocs.io/en/stable/index.html) based on OW. In short, the algorithm
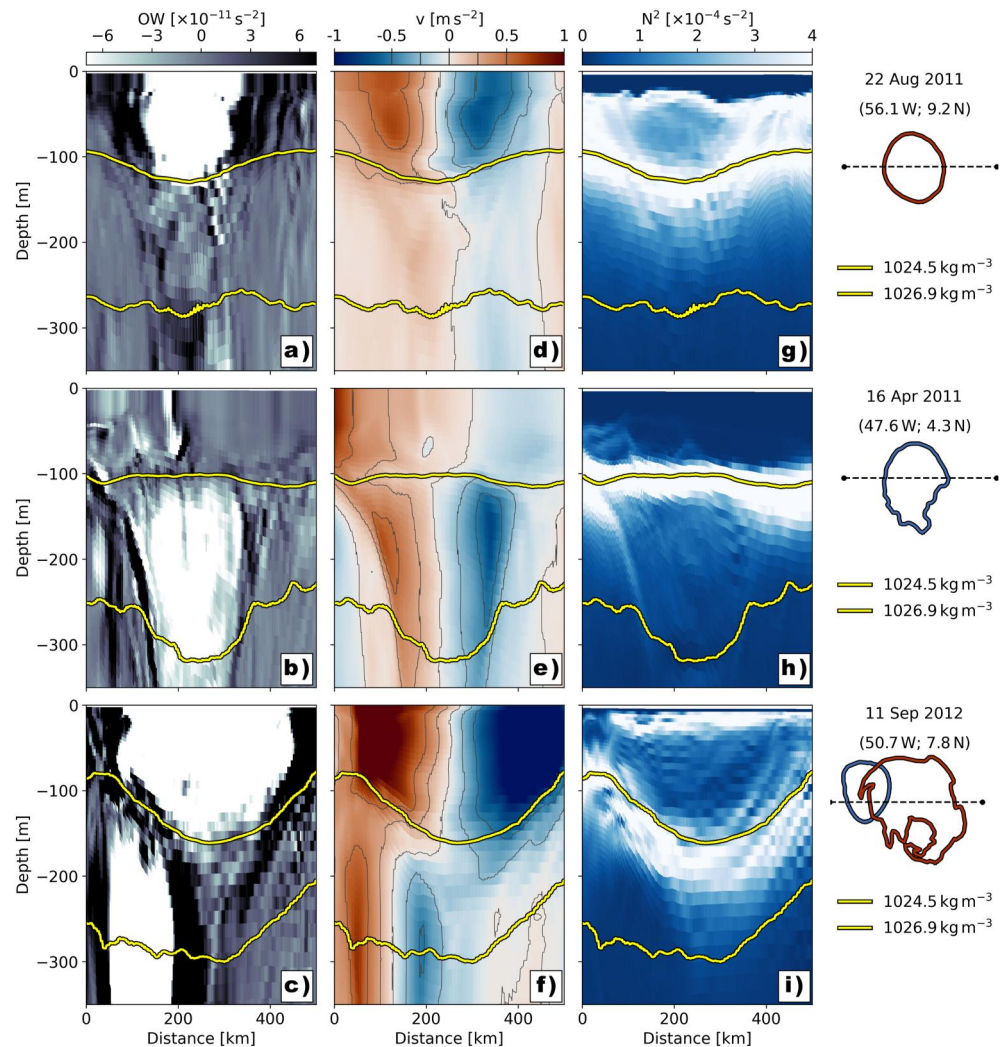
Figure 3. Vertical sections of the NBC rings for the three cases shown in Figure 2. (a–c) Vertical sections of the Okubo-Weiss parameter. (d–f) Vertical sections of meridional velocity v. (g–i) Vertical sections of stratification N^2. Yellow lines represent the 1,024.5 and 1,026.9 kg m^{-3} isopycnals. On the right, red (blue) contours represent the horizontal "x-y" view of the eddy in the vertically averaged layer 1 (2). Coordinates indicate the geographical center of the plot spanning the 500-km section (dashed line).

searches for closed contours of OW in the range $[-1 \times 10^{-9}, -2 \times 10^{-12}]$ with an interval of 2×10^{-12} s^{-2}. We isolate the anticyclones among the identified contours and consider only those with a maximum shape error (deviation from a circle) of 50%. All lateral eddy divisions and mergers are considered as the end and start of associated trajectories. During the tracking phase, we allow linear interpolation of up to six detection gaps (3 days) in trajectories. More details and an animation of OW and eddy identification are provided in Supporting Information S1.

We assume that the northwestward transport of SAW by eddies occurs primarily via large anticyclones (predominantly NBC rings) and thus focus our analyses on these structures. From a recent review of the literature (cf. Subirade et al., 2023), we infer that the typical radius of NBC rings is about 100–200 km. We relax this parameter and consider NBC rings to be the anticyclones that, at some point in their life cycle, have a radius of 80 km. This value represents the mean internal deformation radius for the 2-layer system on the eddy boulevard. It is sufficient to select the NBC rings in layer 1 and the strongest eddies in layer 2, since this lower layer is expected to generate smaller eddies due to a smaller deformation radius than the upper layer and enhanced topographic interaction (e.g., D'Asaro, 1988; Morvan et al., 2019; Napolitano et al., 2020).
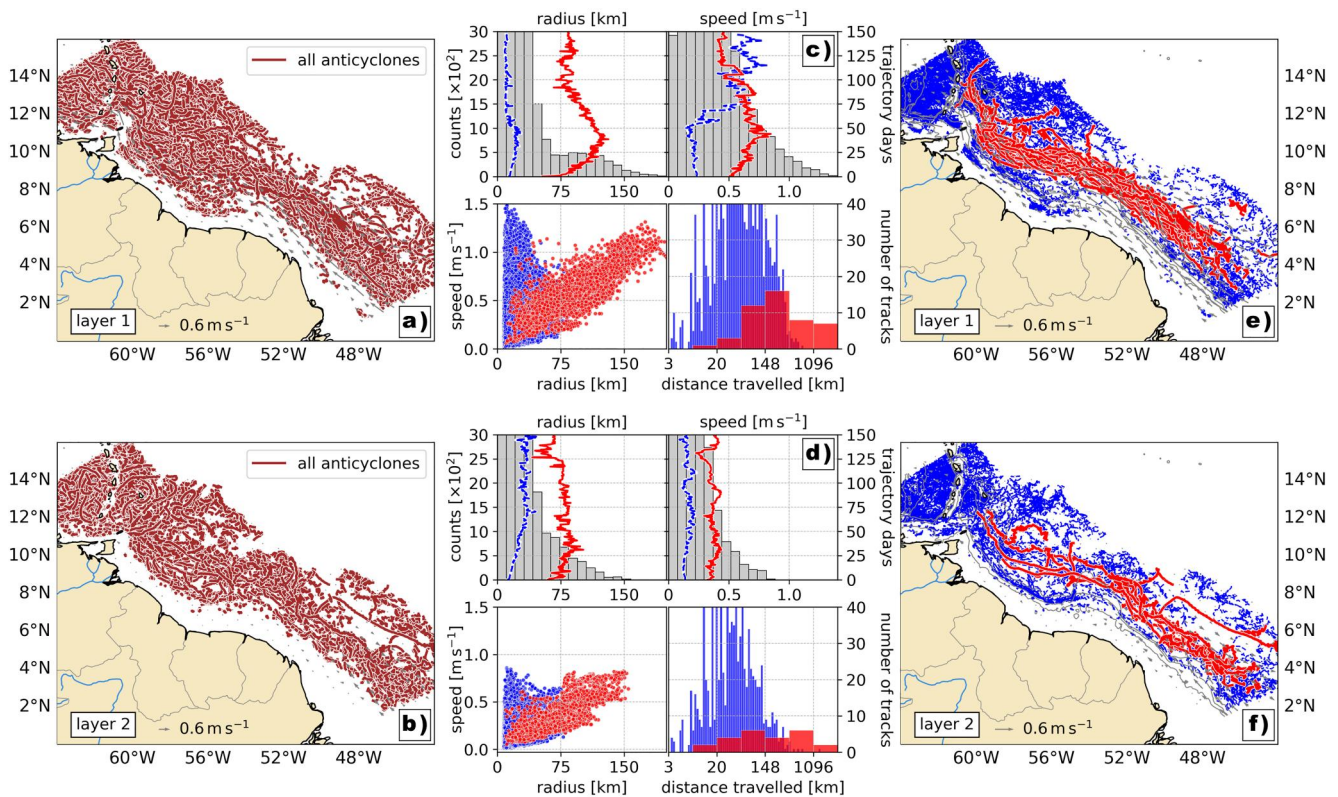
Figure 4. Summary of eddy detections. Model observations and trajectories selected by the 80-km radius threshold are displayed in red and those discarded are displayed in blue. (a–b) Trajectories of all anticyclones for layers 1 and 2. (c–d) Above: statistics of radius and speed versus total counts (bars; left) and days of a median trajectory (lines; right); Below: relation between eddy radius and speed (scatter; left) and distance traveled along the NBC path (bars; right). (e–f) Trajectories of selected and discarded anticyclones for layers 1 and 2.

Eddy detection yielded a total of 59,202 (47,860) anticyclone observations clustered by 3,358 (2,177) trajectories in layer 1(2) during the two years of simulation (Figures 4a and 4b). Using an 80-km radius cut-off, we selected 68 NBC rings in layer 1 and 35 in layer 2 (Figures 4e and 4f). Relaxing the cut-off radius yields more, but relatively smaller NBC rings. For comparison, if we use the mean radius from Subirade et al. (2023) of ~140 km, we get 6 NBC rings generated per year, which is in the ballpark of previous estimates of 5 rings. NBC rings show a fairly linear relationship between radius and speed (Figure 4c). Median values of speed and radius for layer 1 eddies are 0.6 m s^{-1} and 96 km, with maxima of 0.85 m s^{-1} and 120 km respectively. The eddies are first detected with an average radius of 53 km and increase in size and speed until they reach their maximum size 38 days after (about 25% of their lifetime, which roughly agrees with the results in Subirade et al., 2023). Eddy radii slowly decrease toward 75 km by the end of their life cycle. Smaller (<80 km) eddies are numerous and span all velocity ranges, but their northwestward propagation along the eddy corridor rarely exceeds ~200 km, which is approximately the median value for NBC rings (Figure 4c). Therefore, these eddies are not expected to be critical in transporting heat and salt *directly from the formation site*, and we exclude them from the following analyses. In layer 2 (Figure 4d), the radius/speed ratio is also nearly constant for subsurface NBC rings (~75 km, 0.4 m s^{-1}), but there is no apparent growth after their first detection. In addition, the trajectories of selected layer-2 eddies can cover either shorter or longer northwestward distances (Figure 4d), while smaller eddies also rarely propagate more than 200 km. When overlapping, the centers of layer-1 and layer-2 NBC rings can be distant up to ~260 km (80 km in average) from one another.

We now proceed to evaluate the vertical interaction of the NBC rings from our data set of eddy observations and trajectories. To start, pen and paper take the stage as we present the theoretical setup of the problem.

3. NBC Rings Vertical Interaction

3.1. Theoretical NBC Rings

The theoretical background for vertical interaction builds on a series of studies from the early 1990s, which focused on the vertical alignment of vortices and their mutual advection (Hogg & Stommel, 1990). Inspired by newly acquired observations (Käse & Zenk, 1987), Hogg and Stommel (1990) adapted their previous theory on the interaction of baroclinic point vortices (Hogg & Stommel, 1985) to study the interaction of subsurface intensified eddies with surface eddies in the presence of a mean flow. Using a $2\frac{1}{2}$-layer model, the authors showed that the coupling of the two eddies causes advection that depends on the relative vortex strengths. A detailed investigation of vortex alignment followed in Polvani (1991), and the effect of background shear works in tearing this alignment was studied by, for example, Marshall and Parthasarathy (1993). The role of a baroclinic current and its vertical shear in a coherent vortex was revisited by Vandermeirsch et al. (2001, 2002). If vortices are defined by their potential vorticity (PV) anomalies, vortex coherence relies on the strength of these PV patches and their mutual influence; the system will resist and remain coherent as long as the background current shear does not exceed the "coupling velocity" (Vandermeirsch et al., 2002). In the latter study, a top-hat PV distribution was chosen for each layer.

In contrast to some previous studies, we assume that the eddies are initially separated rather than forming a vertically aligned structure. Although eddies are deformed in the realistic model (we allow 50% deformation, see Supporting Information S1), the theory developed here assumes axisymmetric vortices (as does *py-eddy-tracker* for providing radius and velocity estimates). The non-dimensional rotation rate of layer k,

$$\Omega_k(d) = -\frac{1}{d}\sum_n P_k^{(n)}\left[\alpha_1^{(n)}\Delta_1 G^{(n)}(d|r_1) + \alpha_2^{(n)}\Delta_2 G^{(n)}(d|r_2)\right], \tag{2}$$

can be easily converted to a rotational velocity $V_k = d\Omega_k$, where d is the distance separating the eddy center in layer 1 from that in layer 2. The sum of the RHS of Equation 2 represents the combined effects of the first and second baroclinic modes ($n = 1, 2$) of both eddies in layer k. This is essentially controlled by the vertical eigenmodes $\mathcal{P} = P_k^{(n)}$ associated with a stratification matrix $\mathcal{F}$, and consequently by the inversion coefficients $\alpha_k^{(n)} = \mathcal{P}^{-1}$. For each layer k and mode n, the rotation rate depends locally on the eddy PV anomaly Δ_k tampered by a Green function $G^{(n)}$. This function takes the form of a modified Bessel function K_1 or I_1 depending on the magnitude of d compared to the eddy radius r_k. A detailed derivation of Equation 2 and the theory summarized here is given in Vandermeirsch et al. (2001, 2002).

We non-dimensionalized Equation 2 by the upper layer deformation radius R_{d_1} as in Vandermeirsch et al. (2002). Following these authors, we define each layer deformation radius as

$$R_{d_k} = \sqrt{\frac{1}{\gamma_k^2}}, \text{ where}$$

$$\gamma_k^2 = \frac{\Sigma F_i \pm \sqrt{\left(\Sigma F_i^2 - 4(F_1 F_3)\right)}}{2}, \tag{3}$$

with $F_i = F_1, F_2, F_3$ obtained from a $2\frac{1}{2}$-layer framework (see full definitions in Table 1). For the PV anomaly, however, we choose to represent it as the quasi-geostrophic (QG) PV normalized by the planetary vorticity at 4°N (latitude where the eddies usually enter the region), or simply $\Delta_k = \frac{2\zeta_k}{f_{4N}}$. Therefore, as to compare our theoretical results with the numerical model, we re-dimensionalized the velocity by multiplying V_k by the factor $R_{d_1}f_{4N} \approx 1.05$. The complete form of the matrices and functions can be found in Vandermeirsch et al. (2002), but a comparison between the parameters obtained from our numerical simulation to build up the analytical model and their theoretical configuration (though based on typical oceanic conditions) is given in Table 1.

At each occurrence of overlapping eddies, we assess whether these eddies COUPLE into a coherent vortex or ignore each other and remain independent to characterize a SPLIT. Since NBC rings are usually embedded in the (highly-stratified) NBC, which in turn flows along the (steep) continental slope, we neglect the β-effect (cf.

Table 1
List of Parameters Retrieved From GIGATL3 to Build the Theoretical Model in Comparison With the Ones in Vandermeirsch et al. (2002)

Model parameters	GIGATL3 (this study)		Vandermeirsch et al. (2002)
	Layer $k = 1$	Layer $k = 2$	
ρ_k [kg m^{-3}]	1,023.1	1,026.2	—
$g'_{k,k+1}$ [m s^{-2}]	0.030	0.009	0.010/0.005
$<f>$ (2–12°N) [s^{-1}]	1.9×10^{-5}	1.9×10^{-5}	1×10^{-4}
h_k [m]	90	163	500/500
R_{d_k} [km]	105	55	29/12
Nondimensional parameters			
F_k	1.76	0.96	1.7/1.7/3.4
Δ_k	2.3	1.9	1.0/1.0
$P_k^{(n)}$ ($n = 1$)	0.960	0.551	1.7/0.704
$P_k^{(n)}$ ($n = 2$)	0.960	−3.062	1.7/-4.104
$\alpha_k^{(n)}$ ($n = 1$)	0.882	0.277	0.502/0.208
$\alpha_k^{(n)}$ ($n = 2$)	0.159	−0.277	0.086/-0.208

Note. Indices k and n refer to layer number and baroclinic mode, respectively. In the fourth column, Vandermeirsch et al. (2002)'s parameters for layers 1 and 2 are separated by a backslash. The dimensional parameters are density (ρ), reduced gravity (g'), Coriolis parameter (f), layer thickness (h), and layer deformation radius (R_d). The nondimensional parameters are the stratification jump between layers (F), PV anomaly (Δ), vertical eigenmodes of the stratification matrix (P), and inversion coefficients (α). In a $2^1/_2$-layer framework, we consider an infinite layer $k = 3$ with $\rho = 1,027.1$ kg m^{-3} ($F_3 = 3.31$). Note that R_{d_k} is initially calculated at every grid point and then averaged within 70% of the distribution, thus replacing only the mean values of F_i in Equation 3 yields slightly different values.

Vandermeirsch et al., 2002). Therefore, we assume the simplest case of Vandermeirsch et al. (2002): a kinematic split condition

$$\begin{cases} \text{SPLIT}, & \mathbb{U} > V_{1 \leftrightarrow 2} \\ \text{COUPLE}, & \mathbb{U} \leq V_{1 \leftrightarrow 2}, \end{cases} \tag{4}$$

where $\mathbb{U}$ is the background shear and $V_{1 \leftrightarrow 2} = d\Omega_{1 \leftrightarrow 2}$ is again obtained from the rotation rate, this time the one induced by an eddy in the adjacent layer,

$$\Omega_{1 \leftrightarrow 2}(d) = -\frac{1}{d}\sum_n P_1^{(n)} \alpha_2^{(n)} \Delta_2 G^{(n)}(d|r_2)$$

$$- \frac{1}{d}\sum_n P_2^{(n)} \alpha_1^{(n)} \Delta_1 G^{(n)}(d|r_1). \tag{5}$$

As noted in Section 2.1, initially near-barotropic eddies, which are (inaccurately) assumed to be independent, are treated as a special case. When the alignment reaches a critical point, namely a distance $d \simeq 20$ km, the use of the Green function G to describe the eddy velocity leads to a steadily increasing profile (I_1 function) from the center to reach its peak near the eddy boundary, and then a smooth decay (K_1 function) outside of the eddy (cf. Vandermeirsch et al., 2002). For a too small d, the velocity $V_{1 \leftrightarrow 2}$ acting only on the center of each eddy is always weak. Therefore, these nearly aligned structures (which would otherwise show a SPLIT) are classified separately as ALIGNED. In time, these eddies can evolve to a tilted eddy (e.g., Li et al., 2022) and may undergo either coupling or splitting.

The numerical model background vertical shear $\mathbb{U}$ is calculated as follows: for each detected eddy, we project its diameter $2r_k$ (km) zonally and meridionally out of the eddy boundary; then, we remove all the points inside the eddy and average this "background velocity" to obtain a mean vector $U_k = (u_k, v_k)$. We rotate $U_1 = (u_1, v_1)$ by $-\theta$
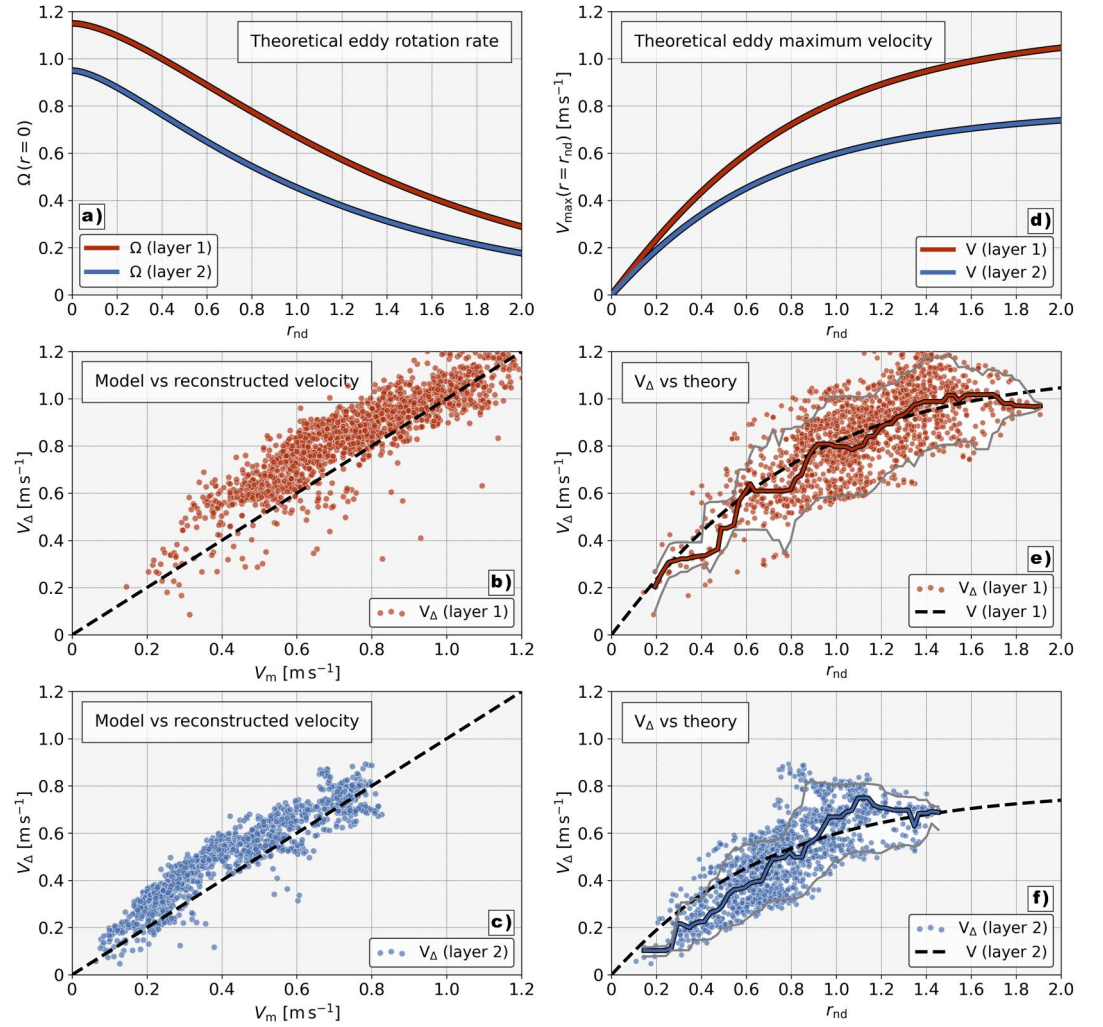
Figure 5. The Vandermeirsch et al. (2002) theoretical eddy for the NBC region. Red and blue colors refer to layers 1 and 2, respectively. (a) Rotation rate at the center of the eddy as a function of the non-dimensional radius r_{nd}. (b, c) Relationship between the theoretical velocity V_Δ and the numerical simulation velocity V_m for layers 1 and 2. The black dashed line represents $V_\Delta = V_m$. (d) Maximum velocity at the eddy edge ($r = r_{nd}$) as a function of r_{nd}. (e, f) V_Δ as a function of r_{nd}. The black dashed line represents the theoretical mean eddy from (d) on the respective layer.

(the angle between U_1 and the origin) so that, by definition, u_1 is positive and $v_1 = 0$. Finally, to preserve the angle between the two vectors, we also rotate $U_2 = (u_2, v_2)$ by $-\theta$ and define the background shear between the layers $k = 1, 2$ as

$$\mathbb{U} \overset{\mathrm{def}}{=} ||-s_{\perp_{|k}}|| = ||-\partial_k u_k + \partial_k v_k|| = \sqrt{(u_1 - u_2)^2 + (v_2)^2}, \tag{6}$$

where u_2 opposite to u_1 increases the shear and the sign of v_2 gives the direction of the normal stress. Flows of different origins that are included in the realistic simulation, such as the NBC, eddy- and topography-induced flows, and internal waves, may affect $\mathbb{U}$. But their arbitrary nature makes it difficult to isolate a "mean current," so the estimate of $\mathbb{U}$ in Equation 6 by definition includes all the above effects averaged together.

The theoretical eddies from Vandermeirsch et al. (2002), built with EUREC4A-OA parameters (Table 1), grow as a function of radius, as also observed for the GIGATL3 eddies (Figure 4). They reach a *plateau* at their maximum speed and minimum rotation rate around $r_{nd} = 2$ (Figures 5a and 5d). In layer 1, the theoretical eddy presents $V_1 = \sim 1 \text{ m s}^{-1}$ at its peak, while in layer 2 $V_2 = 0.8 \text{ m s}^{-1}$. The main differences between our theoretical eddies

and those in Vandermeirsch et al. (2002) are due to the choice of PV normalization and a different value for Δ and F in each layer, which we have chosen to better represent the particularities of our problem. The shape of the eddies, as determined by their radius and the Bessel functions, remains largely unchanged.

Instantaneous observations of overlapping eddies from *py-eddy-tracker* allowed us to evaluate the performance of the theoretical model. We rewrite (2) taking into account the individual information $\epsilon_k = \epsilon_k(r, \Delta)$ of eddies distant $d = d_\epsilon$ from each other. The theoretical velocity V_Δ [m s^{-1}] for each layer as a function of an overlapping pair of eddies (ϵ_1, ϵ_2) becomes:

$$V_\Delta(k) = -f R_{d_1} \sum_n P_k^{(n)} \left[\alpha_1^{(n)} \epsilon_1^{(n)} + \alpha_2^{(n)} \epsilon_2^{(n)} \right],$$ (7)

where the shape of each eddy is given by $\epsilon_k = \Delta_k G(d_\epsilon | r_k)$. Figures 5b and 5c reveals that V_Δ is comparable to the eddy velocity V_m obtained from *py-eddy-tracker*, especially for the stronger eddies. Elsewhere, our reconstruction slightly overestimates the eddy velocity. In Figures 5e and 5f, we compare instances of V_Δ with the mean theoretical eddy.

Having identified the NBC rings in our numerical simulation, we have shown that the theoretical QG model is able to represent these eddies in both layers. Surprisingly (considering the complexity of GIGATL3), and yet anticipated by Vandermeirsch et al. (2002), the simple theoretical QG model captures the overall velocity-radius ratio of the numerical simulation, so that the QG PV anomalies (Δ_k) estimated from V_m can now be used in Equation 5, at the risk of overcounting some coupling events, to investigate the impact of these NBC rings in the adjacent layer. The conditions leading to vertical coupling or splitting between NBC rings and their effects will now be evaluated.

3.2. Eddy Coupling, Splitting, and Effects on Eddy Trajectories

Whenever eddies overlap, their potential coupling or splitting boils down to a competition between the background vertical shear and the velocity imposed by the eddies in the adjacent layer. Remembering Equations 4–6, this "coupling velocity" $V_{1\leftrightarrow2}$ is the sum of the rotation rate $\Omega_{1\leftrightarrow2}$ multiplied by the distance $d = d_\epsilon$ between each eddy of the overlapping pair. And it must be greater than the shear $\mathbb{U}$ between the flow in layers 1 and 2 to characterize a COUPLE event.

According to Vandermeirsch et al. (2002), eddies with $r_{1nd} > 0.5$ can be considered to be split when they no longer overlap. Our criterion for selecting NBC rings (Figure 4) yielded a vast majority of $r_{1nd} > 0.5$ eddies (Figure 5e), so the smaller eddies that could remain vertically coherent without overlap are treated as exceptions and excluded from the analyses. However, we acknowledge that we underestimate possible coupling events for these few smaller eddies. In practice, we only evaluate possible interactions between eddies that (at least) marginally overlap, with a minimum 1% of common points on a ~6 km grid.

To answer our first question—are the NBC ring really independent?—we start, in Figure 6a, with a qualitative evaluation of Equation 4, based on the fairly good agreement between V_Δ and r_{nd} (Figures 5e and 5f). It re-edits the critical shear plot from Figure 5 of Vandermeirsch et al. (2002). Using only the mean theoretical eddy as reference, overlapping eddies are considered to be SPLIT if a point is above the critical shear line (Figure 6a). While Vandermeirsch et al. (2002) point out that strong shear of order 0.1 m s^{-1} can only be found in intense baroclinic jets, $\mathbb{U}$ values in the tropical NBC reach impressive 0.6 m s^{-1}! Under this condition, 862 out of 1,598 interactions are SPLIT, with eddies not affecting the adjacent layer. For example, this evaluation suggests that layer-1 eddies with $r_{nd} < 1$ would most likely always split from the eddies beneath under moderate shear above 0.2 m s^{-1}.

If on the one hand, the previous statement seems vague and qualitative, on the other hand, it has important consequences: since speed and radius are correlated, we can expect that NBC rings with $r_{nd} \leq 1$ in a background shear of $\gtrsim 0.2$ m s^{-1} are indeed shallow NBC rings with no subsurface counterpart. For present calculations of inter-hemispheric heat and salt transport based on a mean NBC ring depicted by SSH (e.g., Bueno et al., 2022), this could represent an important bias for future estimates based on forthcoming higher resolution SSH products that will allow the detection of smaller structures (e.g., SWOT, Morrow et al., 2019). However, the analysis of couple and split based solely on a critical line from the mean theoretical eddy does not correctly account for aligned eddies—see the 104 occurrences randomly distributed throughout the scatter cloud (Figure 6a).
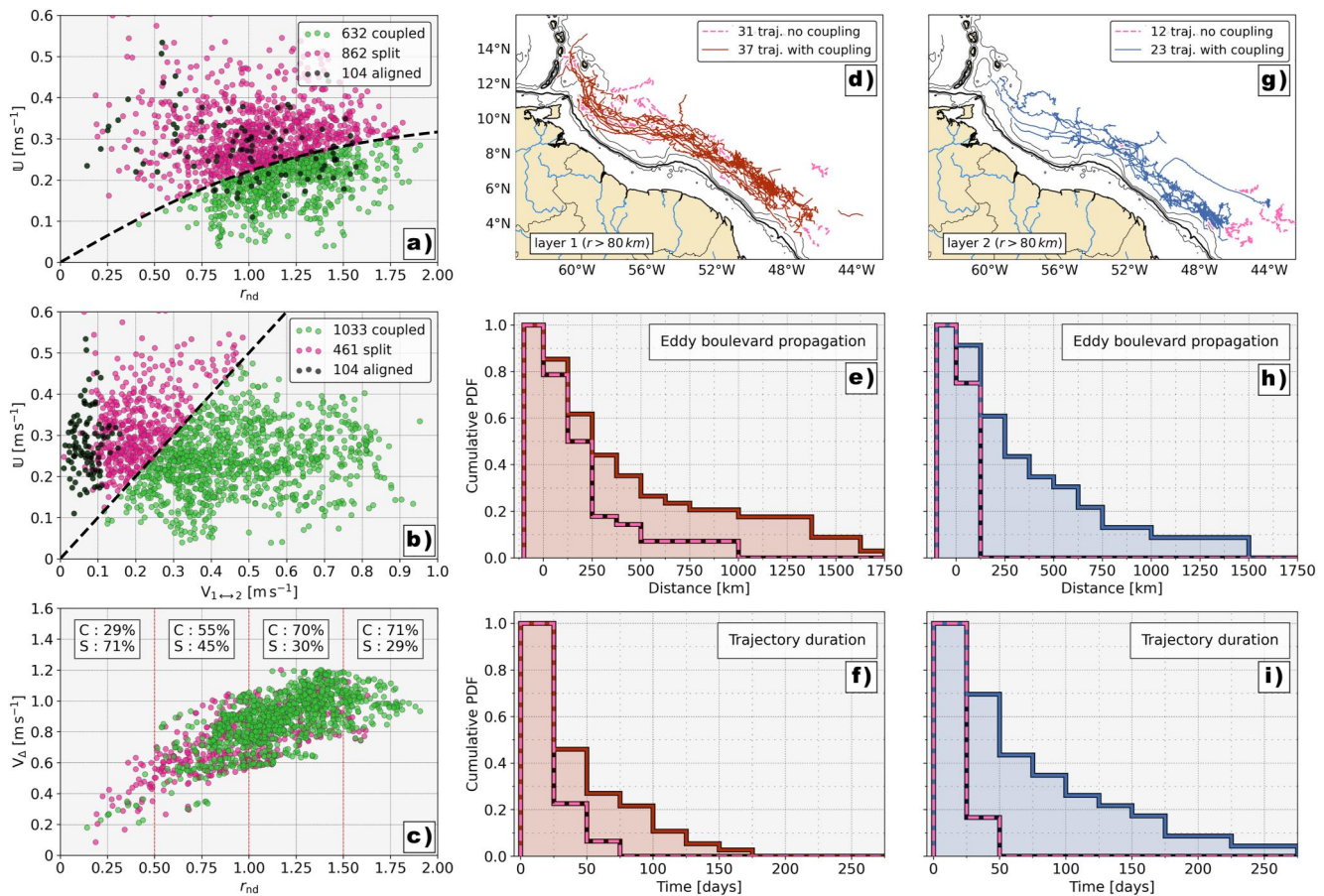
Figure 6. Evaluation of coupling and splitting events for GIGATL3. (a) Coupled (green), split (pink), and aligned (black) eddy pairs based on the mean theoretical eddy and critical shear (black dashed line). (b) Coupled (green), split (pink), and aligned (black) eddy pairs based on the direct comparison of the velocity in the adjacent layer and the background shear. The black dashed line now represents the critical condition $\mathbb{U} = V_{1 \leftrightarrow 2}$. (c) Results of the critical condition in (b), expressed in terms of layer 1 eddies' velocity and radius. The effect of coupling on layer 1 and 2 eddies is shown in terms of coupled and non-coupled (split) for the eddies' trajectories (d, g), northwestward propagation (e, h), and duration (f, i). The black thick line in (d, g) represents the 300 m isobath.

Figure 6b displays a more quantitative condition, a pointwise comparison between $\mathbb{U}$ and $V_{1 \leftrightarrow 2}$. This direct evaluation can correctly classify unusually large-but-slow eddies that may split under moderate shear, and conversely, the small-but-fast eddies that may remain coupled under higher shear conditions. Here, 461 SPLIT cases indicate a large underestimation of coupling by the qualitative method (note that the 461 SPLIT cases are *not necessarily* included in the 862 SPLIT cases from Figure 6a). In Figure 6b, accessing the special cases where $d < 20$ km indeed shows ALIGNED eddies grouped under "split conditions," with weaker $V_{1 \leftrightarrow 2}$ from Equation 5. Thus, as defined, COUPLE is only possible on eddies distant $d \geq 20$ km from one another (our first COUPLE appears with $d \sim 22$ km, even in low shear conditions).

The relationship between the eddies and the background environment is better seen in Figure 6c, which shows the direct couple-split evaluation as a function of layer-1 eddies radius and velocity. Considering that the $\mathbb{U}$ distribution is more or less homogeneous for all eddy radii (Figure 6a), coupling naturally increases with eddy radius and velocity; for $r_{nd} < 1$, splitting accounts for about 70% of the interactions, consistent with the qualitative evaluation in Figure 6a. Coupling becomes more important as eddies get stronger, but still account for no more than $\sim 70\%$ of the interactions for $r_{nd} > 1$ eddies. In practice, it means that a relatively large ($r_{nd} > 1$) NBC ring has a 30% chance of being a SPLIT (i.e., confined to the TW layer). Therefore, even considering only overlapping eddies, to assume that surface NBC rings would always extend to depths of ~ 300 m is to run the risk of over-estimating the *subsurface* transport of SAW by about a third!

It is worth recalling that, in our theoretical setup, the depth of layer 2 extends only to the SACW lower boundary. Considering the whole extent of subsurface-intensified eddies could change h_2 and $g_{2,3}$, decreasing F_2 and F_3 (see

Table 1, and derivation in Vandermeirsch et al., 2002) and increasing $V_{\Delta 2}$ (Figures 5c and 5f), as well as chances of coupling. However, the vertically-averaged PV anomaly Δ_2 would likely be weaker for deeper eddies, leaning the system toward splitting. A detailed study on the vertical structure of NBC rings and its consequences for coupling is needed.

So far, we have considered the coupling or splitting between eddies in an isolated context. However, if the present processes are to be linked to the transport of SAW into the North Atlantic subtropical gyre, they must affect the northwestward propagation of NBC rings along the continental margin. Given that interacting eddies can COUPLE or SPLIT, we now know that although the NBC rings coexist independently (e.g., Stevens et al., 2021), they are capable of coupling and propagating as a pair.

By tracing all interaction events back to the original trajectories of the eddies selected by *py-eddy-tracker* (Figure 4), we classify the trajectories into those in which at least one coupling event occurred and those in which no coupling was detected (either by no overlapping of eddies or by overlapping with SPLIT only). Figure 6d shows the 68 layer-1 trajectories, divided into 37 with coupling and 31 without. Their distribution is fairly homogeneous along the eddy boulevard, with both types of trajectory seemingly undisturbed by the presence or absence of coupling. Clustering these trajectories by the distance traveled along the eddy boulevard (Figure 6e) and their lifetime (Figure 6f), the statistics suggest that although the lifetime and propagation increase under coupling, such events do not seem to affect these trajectories much. In fact, 50%–60% of all trajectories travel about 250 km; this number drops by half for the next 250 km, and while 10% of the eddies travel up to 1,000 km without coupling, only about 20% do so with coupling (Figure 6e). Coupling can double the lifetime of a few eddies, but whether coupled or not, trajectories in layer 1 rarely exceed 150 days (Figure 6f; Fratantoni et al., 1995), with eddies rapidly navigating the eddy boulevard to be destroyed downstream as they enter the Caribbean islands region (e.g., Andrade-Canto & Beron-Vera, 2022; Fratantoni & Glickson, 2002).

The situation of the 35 trajectories in layer 2 (Figure 6g) is more peculiar. There, 60% of the trajectories that travel 250 km do so only in the presence (at any given time) of coupling with the eddies in layer 1 (Figure 6h). Without coupling, layer 2 eddies travel a maximum of 125 km and barely survive more than 25 days (Figure 6i). However, coupled layer-2 eddies acquire the long lifetimes and large displacements of SCVs, even longer than the layer-1 eddies to which they are coupled. About 40% of the coupled subsurface eddies travel 500 km, with ∼10% carrying SAW for 1,500 km over 200 days to reach the Caribbean islands—see the longest trajectories in Figure 6g. We also find that most of the uncoupled trajectories in layer 2 occur at the entrance of the eddy boulevard. This region of accumulating vorticity often leads to lateral merging and division of eddies (Subirade et al., 2023, see also Movie S1). Adding these processes to our analyses could alter our results in the sense that the uncoupled trajectories could be unified as a "child" trajectory of the longer ones. Nevertheless, such lateral interactions break the coherence of the eddies (e.g., de Marez, Carton, L'hégaret, et al., 2020), allowing initially trapped SAW to potentially spread within the eddy boulevard and mix with local North Atlantic waters.

We have learned that eddies interact vertically within the eddy boulevard. While overlapping, the two-way velocity that eddies impose on each other is often important to outmatch stratification and COUPLE both layers. Locally, coupling appears to increase the duration of eddies, notably at subsurface, allowing them to propagate over longer distances than in the absence of coupling. On a larger scale, local coupling could lead to SAW eddies reaching the Caribbean sea. But, if we recall Figure 2a, we first noticed these subsurface eddies as quasi-standing features, except for the rogue trajectories that stood out among the OW of layer 1. This means that, especially for layer 2, increasing lifetime does not necessarily mean that eddies propagate over longer distances. So why does there seem to be a link between eddy coupling, lifetime, and propagation for layer 2 (Figures 6g–6i)?

In the following section, we seek answers to this question by revisiting the Hovmöller diagram of the eddy boulevard (Figure 2), now showing the coupling and splitting events superimposed on the OW tracks and their spatial distribution.

3.3. Coupling and Splitting Throughout the Eddy Boulevard

The Hovmöller diagram in Figure 7 shows, as expected, the overlapping bands of OW from layers 1 and 2 indicating moments of interaction between the surface and subsurface eddies. Indeed, Figure 7a shows coupling and splitting events populating the strong OW signal of the longest trajectories. In general, eddies first COUPLE around 5°N (∼500 km in Figure 7a). However, during the vertical alignment process, the NBC rings can also
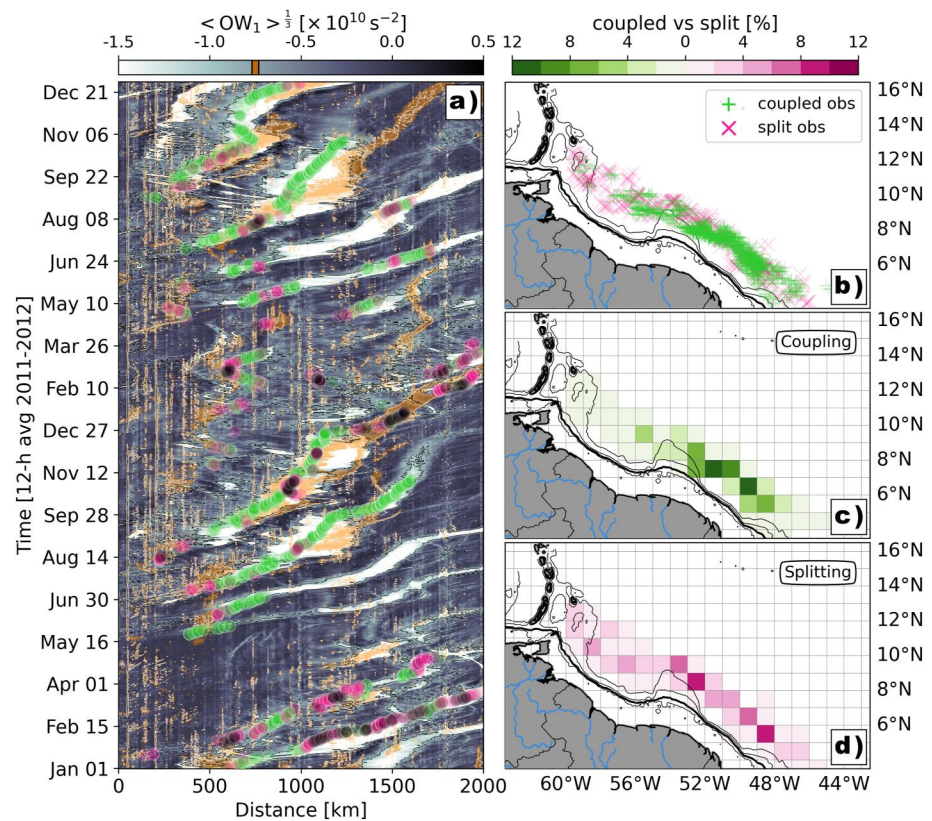
Figure 7. (a) Hovmöller diagram of $<OW_1>^{1/3}$ with superimposed dots showing coupling (green dots), splitting (pink dots), and alignment (black dots) events. Orange bands show $<OW_2>^{1/3}$ values stronger than an arbitrary threshold -7.5×10^{-11}. (b) Spatial distribution of coupling (green +) and splitting (pink x) events along the eddy boulevard. (c, d) Spatial distribution of the percentage of coupling and splitting in a $1° \times 1°$ grid. The black thick line represents the 300 m isobath.

interact with other eddies arriving in the region, leading to a competition between vertical and horizontal interaction. Moreover, the alignment process by coupling is often very slow (e.g., Nof & Dewar, 1994), which could also explain some bypassing surface rings that briefly interact with the subsurface quasi-standing rings but continue alone on their northwestward path, eventually interacting with other structures far downstream (examples are clearly seen in Figure 7a, on May 2011 and 2012). Those eddies that manage to remain coupled often detangle from the "quasi-standing" NBC retroflection (e.g., Silveira et al., 2000) and propagate northwestward as a pair.

Although resilient in many cases, a COUPLE is never definitive for eddies traveling as pairs, but an alternation between coupling and splitting is often observed, indicating the subtlety of the process when observed at relatively high frequency (12 hr in the present work). When analyzing the vertical alignment with a realistic model, there are variables that are beyond our control, such as changes in eddy size along the trajectories, which can occur within each layer due to lateral shear and interaction with other eddies and/or topography. Indeed, some of the SPLIT detected over previously coupled eddies that continue to propagate in the same direction follow a disappearance of the OW signal in Figure 7a—e.g., 01 Jan 2011 for layer 2 and 27 Dec 2011 for layer 1—indicating that the eddy in these layers has become weaker and/or smaller. Moreover, the sensitivity of Equation 4 defining the interaction also deserves attention, since $\mathbb{U}$ itself is a non-trivial estimate, and the more the eddies are aligned on the vertical, the shorter the distance d_ϵ becomes, leading to $V_{1 \leftrightarrow 2} \simeq 0$, and ultimately a SPLIT. To mitigate this effect, we have introduced the ALIGNED classification. The trajectories that show a greater alternation between coupling and splitting also show eddies closely aligned with their counterparts (black dots on Figure 7a), where eddies can propagate in an oscillating state around a stationary vorticity configuration (a V-state, cf. Polvani, 1991), cycling through different values of d and shifting instances of COUPLE, SPLIT, and ALIGNED.

To address the implications of coupling for the lower-layer eddies within the present framework, the time-independent spatial distribution of coupling and splitting is shown in Figure 7b. Grouping these events unveils an interesting pattern that complements the NBC rings interaction story: splitting is scattered throughout the domain, suggesting that there is no local control other than $\mathbb{U}$ and its various components [see discussion around Equation 6] driving overlapping trajectories to SPLIT (Figure 7c). Coupling, in turn, is more concentrated in the first half of the eddy boulevard, with 80% of COUPLE occurring east of 53°W (Figure 7d), notably upstream of the topographic choke point that lies in the path of layer 2, as if bound to happen in this region. (Recalling the vertical section along the eddy boulevard Figure 1, layer 2 is almost blocked by a topographic bump along the main NBC axis, located immediately downstream of the retroflection region.) When both layers are recirculating (Bourlès et al., 1999; Goes et al., 2005; Silveira et al., 2000), layer-1 eddies develop slightly to the west of layer-2 eddies (see e.g., Metcalf & Stalcup, 1967, and the Movie S1); nevertheless, the two newly formed eddies are often close enough to begin interacting, as simulated by for example, Polvani (1991) and Reinaud and Carton (2020), reproduced by Nof and Dewar (1994), and observed for Mediterranean-water eddies by Tychensky and Carton (1998). At this point, overlapping NBC rings tend to align vertically, giving the green light for their interaction, which can generate a net advection on each other if the eddies are strong enough to COUPLE (Vandermeirsch et al., 2001).

Vertical interaction between layers has previously been reported along the non-trivial western boundary current regime off the Brazilian continental margin. Silveira et al. (2008, 2023) detail the growth of the quasi-standing cyclonic meanders off southeastern Brazil, driven by the vertical interaction of the opposing flows of the Brazil Current (BC) and the Intermediate Western Boundary Current (IWBC). Upstream on the BC path, at 20°S, Napolitano et al. (2021) suggest, using a theoretical model, that the local meandering of the BC that gives rise to the Vitória Eddy (Schmid et al., 1995) is driven by vertical interaction with a topographically constrained IWBC eddy. In all of these regions, the meanders can occasionally shed coherent eddies that are then free to propagate away from the growth region. These processes could also be a consequence of the interaction of the layers (Arruda et al., 2013; Mill et al., 2015). In the equatorial NBC-NBUC domain, the Barreirinhas eddies were found to be vertically independent features formed in a highly stratified region, with Burger number $Bu = \left(\frac{R_d}{r_1}\right)^2 \sim 10$ (Simoes-Sousa et al., 2021). For the NBC rings further downstream in the NBC retroflection region, relaxation of the stratification yields $Bu \sim 1$. This value was previously estimated by Krelling et al. (2020) for comparison with the authors' description of the Potiguar Eddy, a mesoscale subsurface eddy trapped by the topography near (37°W; 4°S), which gives $Bu = 0.97$. In such structures, rotation and stratification go hand in hand, allowing for rich interactions (Cushman-Roisin & Beckers, 2011), such as vertical coupling.

3.4. Does Vertical Coupling Between NBC Rings Matter for the Export of South Atlantic Water?

Both the alignment process by coupling and the propagation of coupled eddy pairs, as observed in the literature, depend on the ratio between the eddy radius and the baroclinic deformation radius. This ratio, studied in detail by Polvani (1991), can set the tone for the dynamics of the interaction. For small Bu, that is, $r_1 > R_d$, the initial 2-layer baroclinic configuration acquires an essentially barotropic configuration during alignment. In our case, this would imply a shift from a $2\text{-}^1/_2$ layer to an equivalent barotropic configuration, which is also more suitable for the case of NBC rings (compared to the barotropic case) and favors advection by the mean flow (e.g., Klocker & Marshall, 2014; Napolitano et al., 2019). Smaller eddies, with $r_1 \approx R_d$ may start to align depending on the initial distance d_e, but will eventually reach a V-state (Polvani, 1991). For the simulated NBC rings, the dynamics are even more complex, since $r_1 > R_d$ can coexist and interact with $r_2 < R_d$ eddies (and vice-versa). We observed, in one COUPLE event, a subsurface NBC ring trajectory with an oscillating pattern around a much larger surface NBC ring as it propagated northwestward (not shown). Further analyses are required to understand their dynamics in complex simulations.

Thus, armed with a simple theoretical model, we can but speculate that layer-2 eddies may be driven by their surface accomplices to move offshore and around the topographic bump. Once coupled, the structure may behave as a tilted eddy (e.g., Li et al., 2022), which sets up a baroclinic current that advects the eddy pair (e.g., Vandermeirsch et al., 2001; Walsh et al., 1996). In more complex interactions, propagation can result from the formation of V-state dipoles (Polvani, 1991). Constrained by topography to the northwest—the primary direction for NBC rings translation (e.g., Fratantoni & Glickson, 2002)—the interaction of the eddies with the continental slope will lead them to circumvent the bump (the "mirror effect"; e.g., X. Carton et al., 2013). Free from this

topographic choke point, layer-2 eddies are then able to propagate northwestward as a pair, or even on their own, as seen in the lone layer-2 eddy on 2012 Nov 06, after stopping to overlap with the surface eddy at about 1,250 km (Figure 7a). If unable to COUPLE with the surface, layer-2 eddies do not propagate along the eddy boulevard, condemned to remain within the NBC retroflection under the influence of the curvature of the flow (e.g., Buckingham et al., 2021a, 2021b, see also the long-lived, quasi-standing, layer-2 eddies in Figure 7a) and topographic stress (e.g., X. Carton & Legras, 1994) which could act to stabilize the eddy, and merging with other structures that could break it (e.g., Ciani et al., 2016).

The ability to couple and move past topography seems critical to the northwest transport of SAW, notably at subsurface, where the SACW carried by these eddies represent most of the SAW (e.g., Johns et al., 2003; Kirchner et al., 2009). To illustrate this effect, we estimate the transport of SAW by NBC rings in both layers. We follow the concept of annualized eddy transport from Johns et al. (2003) to obtain the total transport Φ_{SAW} (Equation 8). We multiply the number of trajectories nt by the annualized mean eddy transport,

$$\Phi_{SAW}(k) = nt \, \frac{\overline{\Phi_k}}{\Delta T} = \frac{nt}{\Delta T} \frac{1}{m} \sum_{1}^{m} \underbrace{\pi \, r_k^2 \, h_k}_{\Phi_k} , \tag{8}$$

with an annualized ($\Delta T = 1$ year) cylindrical NBC ring described by r_k and h_k (obtained from *py-eddy-tracker*) for each $m = [1,2\ldots,m]$ detection in 1° longitude bins for the extension of the eddy boulevard.

Figures 8a and 8b show the total volume transport by NBC rings along the eddy boulevard for trajectories with or without coupling. We note that there are few interactions upstream of 48°W due to different locations for ring generation in the two layers. (e.g., Metcalf & Stalcup, 1967). When trajectories SPLIT (or no overlap occurs at all), surface NBC rings pass over the bump carrying SAW toward the northwest, as illustrated in Figures 8c–8e. (We recall that SAW, particularly at the surface, is locally mixed with North Atlantic waters, e.g., Hellweger & Gordon, 2002, but we do not consider such process for the current estimate). For trajectories with coupling, SAW peaks around 49°W (Figure 8b), within the strip of the eddy corridor where coupling is maximum (Figure 7b). Past the topographic bump at 52°W, 1.5–2.5 Sv of SAW is conveyed northwestward by the combined effect of surface and subsurface eddies (Figure 8b), which is consistent with previous estimates of annualized transport of <1 Sv for <300-m depth NBC rings (Johns et al., 2003; Subirade et al., 2023) multiplied by the number of trajectories nt. As mentioned above, we suggest that coupling is optimal when eddies approach the topographic bump between 48 and 52°W, and eddies circumvent the bump as a pair (see a schematic representation in Figures 8f–8h).

Even over steep topographic slopes, NBC rings are usually not destroyed by the emission of topographic waves (Jacob et al., 2002; LaCasce, 1998). Closer to the surface, these eddies propagate northwestward under the combined influence of the β effect and the continental margin orientation (Fratantoni & Glickson, 2002; Fratantoni & Richardson, 2006; Jacob et al., 2002), with the possible influence of advection by the NBC (e.g., Klocker & Marshall, 2014) and wobbling driven by lateral interaction with other eddies, notably cyclones (e.g., Deremble et al., 2016). However, in the subsurface, not only are eddies blocked by the topography, but most of the NBC lower-layer flow retroflects to the east (e.g., Goes et al., 2005); the remaining local currents and other small eddies (cyclones) are weak and generally unable to influence larger subsurface NBC rings, creating a quasi-standing region. Along the Brazilian continental margin, the trapping of recirculation-driven subsurface eddies by topography has been observed for the IWBC eddy (Napolitano et al., 2019) and the Potiguar eddy (Krelling et al., 2020). At the surface, the Vitória eddy and São Tomé eddy grow as cyclonic meanders of the BC, with northward translation events associated with interactions between the eddies and the lower layer flow (i.e., the IWBC, Campos, 2006; Mill et al., 2015). Therefore, the idea that coupling with the surface NBC rings allows the subsurface eddies to bypass this topographic obstacle and detach from the retroflection region explains the link between the coupling effect and the observed increase in both lifetime and distance traveled. With many simultaneous processes occurring, this idea comes forth rather as a *necessary* condition than a *sufficient* one. We call out for follow-up studies to observe and elucidate these processes.

4. Final Remarks

In his seminal description of SCVs in 1985, McWilliams compared their coherent behavior to that of the coherence of the "Amazon freshwater outflow eddies," later dubbed NBC rings (Johns et al., 1990). Recent
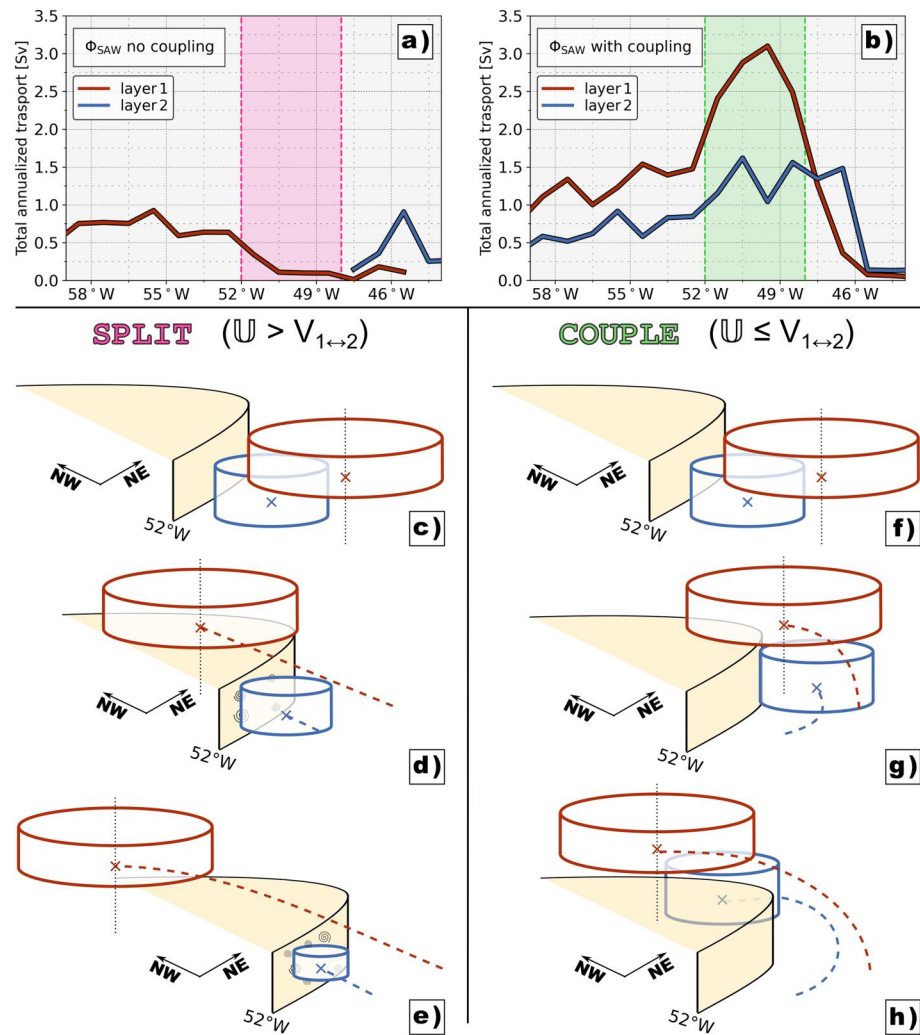
Figure 8. (a, b) SAW total annualized transport by surface (red lines) and subsurface (blue lines) NBC rings for the 2-year model period. The hashed areas indicate the bands of high SPLIT (a) and COUPLE (b) according to Figure 7c upstream of the topographic bump drawn in panels (c–h). Schematics of the suggested relationship between NBC rings and the topography in layers 1 (red) and 2 (blue) during SPLIT (c–e) and COUPLE (f–h) events. Dotted lines indicate possible ring trajectories over and around the bump.

observations (Stevens et al., 2021) have also confirmed the presence of smaller, subsurface-intensified NBC rings. In the present study, we show that surface and subsurface intensified NBC rings not only coexist, but also interact vertically, with subsurface NBC rings acquiring characteristics of SCVs such as increased propagation and lifetime and with surface NBC rings playing a key role in the process.

Inheriting independent cores from the upstream NBC-NBUC system, NBC rings tend to develop independently within the Tropical Water (near-surface, with North Atlantic characteristics) and the South Atlantic Water (essentially the subsurface Maximum Salinity Water and the pycnocline South Atlantic Central Water) layers, although they often overlap in their formation region, the NBC retroflection. This overlap can lead to the coupling of the two layers and mutual advection of the eddies therein. Using a simple quasi-geostrophic theoretical eddy model, we were able to reproduce the NBC rings shown in a realistic numerical simulation.

Applying a kinematic condition for the coupling or splitting of the pairs of eddies reveals that a SPLIT, although less common, can basically occur anywhere in the domain, driven either by strong background shear or by weak eddy interaction. Coupling in turn is concentrated in the region upstream of a topographic choke point. Despite some influence, coupling does not appear to have a major effect on the shallow NBC rings. However, it is crucial for the

propagation and lifetime of the subsurface NBC rings. While surface eddies can detach from the retroflection region and propagate northwestward undisturbed, we suggest that subsurface eddies depend on coupling with the surface to leave the retroflection region. Due to coupling, these rings navigate past the topographic bump that constrain their path to reach the westernmost portions of the eddy boulevard, transporting SAW into the Caribbean sea (through their demise when facing the islands; Fratantoni & Richardson, 2006; McWilliams, 1985; Subirade et al., 2023) and connecting the southern and northern subtropical gyres.

Besides recent advances in the AMOC studies with new data and satellite-based products (e.g., Bueno et al., 2022; Chidichimo et al., 2023; Tuchen et al., 2022), the vertical structure and dynamics of NBC rings in different layers is still a challenge that needs to be further addressed to improve the assessment of the AMOC cross-hemispheric transport and to further develop future climate predictions. Diagnostics such as those presented here have caveats resulting from the application of a QG-based theory to a numerical simulation, that, like any other model, has its own limitations. Nevertheless, they provide important base knowledge and invite researchers to build on it with further analyses and observations.

Data Availability Statement

The source code of the simulation used in this study is available at https://doi.org/10.5281/zenodo.4948523 (Gula et al., 2021). Animation (Movie S1) and the tutorial code for eddy tracking and model files for a minimal example (described in Supporting Information S1) can be obtained at https://doi.org/10.5281/zenodo.10636521 (Napolitano et al., 2024). The Napolitano et al. (2024) data set also contains all the trajectory files of identified anticyclones used in this study and the analysis results of coupling and splitting for overlapped eddies.

References

Andrade-Canto, F., & Beron-Vera, F. (2022). Do eddies connect the tropical Atlantic Ocean and the Gulf of Mexico? *Geophysical Research Letters*, *49*(20), e2022GL099637. https://doi.org/10.1029/2022GL099637

Arruda, W. Z., Campos, E. J., Zharkov, V., Soutelino, R. G., & Silveira, I. C. (2013). Events of equatorward translation of the Vitoria Eddy. *Continental Shelf Research*, *70*, 61–73. https://doi.org/10.1016/j.csr.2013.05.004

Becker, J., Sandwell, D., Smith, W., Braud, J., Binder, B., Depner, J., et al. (2009). Global bathymetry and elevation data at 30 arc seconds resolution: Srtm30_plus. *Marine Geodesy*, *32*(4), 355–371. https://doi.org/10.1080/01490410903297766

Bosse, A., Testor, P., Mortier, L., Prieur, L., Taillandier, V., d'Ortenzio, F., & Coppola, L. (2015). Spreading of Levantine Intermediate Waters by submesoscale coherent vortices in the northwestern Mediterranean Sea as observed with gliders. *Journal of Geophysical Research: Oceans*, *120*(3), 1599–1622. https://doi.org/10.1002/2014JC010263

Bourlès, B., Molinari, R., Johns, E., Wilson, W., & Leaman, K. (1999). Upper layer currents in the western tropical north Atlantic (1989–1991). *Journal of Geophysical Research*, *104*(C1), 1361–1375. https://doi.org/10.1029/1998JC900025

Buckingham, C. E., Gula, J., & Carton, X. (2021a). The role of curvature in modifying frontal instabilities. Part II: Application of the criterion to curved density fronts at low Richardson numbers. *Journal of Physical Oceanography*, *51*(2), 317–341. https://doi.org/10.1175/JPO-D-20-0258.1

Buckingham, C. E., Gula, J., & Carton, X. (2021b). The role of curvature in modifying frontal instabilities. Part I: Review of theory and presentation of a nondimensional instability criterion. *Journal of Physical Oceanography*, *51*(2), 299–315. https://doi.org/10.1175/JPO-D-19-0265.1

Bueno, L. F., Costa, V. S., Mill, G. N., & Paiva, A. M. (2022). Volume and heat transports by North Brazil Current rings. *Frontiers in Marine Science*, *9*, 831098. https://doi.org/10.3389/fmars.2022.831098

Campos, E. J. (2006). Equatorward translation of the Vitória Eddy in a numerical simulation. *Geophysical Research Letters*, *33*(22), L22607. https://doi.org/10.1029/2006GL026997

Carton, J. A., & Giese, B. S. (2008). A reanalysis of ocean climate using simple ocean data assimilation (SODA). *Monthly Weather Review*, *136*(8), 2999–3017. https://doi.org/10.1175/2007MWR1978.1

Carton, X., Le Cann, B., Serpette, A., & Dubert, J. (2013). Interactions of surface and deep anticyclonic eddies in the Bay of Biscay. *Journal of Marine Systems*, *109*, S45–S59. https://doi.org/10.1016/j.jmarsys.2011.09.014

Carton, X., & Legras, B. (1994). The life-cycle of tripoles in two-dimensional incompressible flows. *Journal of Fluid Mechanics*, *267*, 53–82. https://doi.org/10.1017/S0022112094001114

Chidichimo, M. P., Perez, R. C., Speich, S., Kersalé, M., Sprintall, J., Dong, S., et al. (2023). Energetic overturning flows, dynamic interocean exchanges, and ocean warming observed in the South Atlantic. *Communications Earth & Environment*, *4*(1), 10. https://doi.org/10.1038/s43247-022-00644-x

Ciani, D., Carton, X., & Verron, J. (2016). On the merger of subsurface isolated vortices. *Geophysical & Astrophysical Fluid Dynamics*, *110*(1), 23–49. https://doi.org/10.1080/03091929.2015.1135430

Cushman-Roisin, B., & Beckers, J.-M. (2011). *Introduction to geophysical fluid dynamics: Physical and numerical aspects*. Academic press.

Dai, A., & Trenberth, K. E. (2002). Estimates of freshwater discharge from continents: Latitudinal and seasonal variations. *Journal of Hydrometeorology*, *3*(6), 660–687. https://doi.org/10.1175/1525-7541(2002)003⟨0660:EOFDFC⟩2.0.CO;2

D'Asaro, E. A. (1988). Generation of submesoscale vortices: A new mechanism. *Journal of Geophysical Research*, *93*(C6), 6685–6693. https://doi.org/10.1029/JC093iC06p06685

de Marez, C., Carton, X., Corréard, S., L'Hégaret, P., & Morvan, M. (2020). Observations of a deep submesoscale cyclonic vortex in the Arabian Sea. *Geophysical Research Letters*, *47*(13), e2020GL087881. https://doi.org/10.1029/2020GL087881

de Marez, C., Carton, X., L'hégaret, P., Meunier, T., Stegner, A., Le Vu, B., & Morvan, M. (2020). Oceanic vortex mergers are not isolated but influenced by the β-effect and surrounding eddies. *Scientific Reports*, *10*(1), 2897. https://doi.org/10.1038/s41598-020-59800-y

Deremble, B., Dewar, W. K., & Chassignet, E. P. (2016). Vorticity dynamics near sharp topographic features. *Journal of Marine Research*, *74*(6), 249–276. https://doi.org/10.1357/002224016821077170

Dong, C., McWilliams, J. C., Liu, Y., & Chen, D. (2014). Global heat and salt transports by eddy movement. *Nature Communications*, *5*(1), 3294. https://doi.org/10.1038/ncomms4294

Fratantoni, D. M., & Glickson, D. A. (2002). North Brazil Current ring generation and evolution observed with SeaWiFS. *Journal of Physical Oceanography*, *2*(3), 1058–1074. https://doi.org/10.1175/1520-0485(2002)032⟨1058:NBCRGA⟩2.0.CO;2

Fratantoni, D. M., Johns, W. E., & Townsend, T. L. (1995). Rings of the North Brazil Current: Their structure and behavior inferred from observations and a numerical simulation. *Journal of Geophysical Research*, *100*(C6), 10633–10654. https://doi.org/10.1029/95JC00925

Fratantoni, D. M., & Richardson, P. L. (2006). The evolution and demise of North Brazil Current rings. *Journal of Physical Oceanography*, *36*(7), 1241–1264. https://doi.org/10.1175/JPO2907.1

Fu, L.-L., Chelton, D. B., Le Traon, P.-Y., & Morrow, R. (2010). Eddy dynamics from satellite altimetry. *Oceanography*, *23*(4), 14–25. https://doi.org/10.5670/oceanog.2010.02

Goes, M., Molinari, R., da Silveira, I., & Wainer, I. (2005). Retroflections of the North Brazil Current during February 2002. *Deep Sea Research Part I: Oceanographic Research Papers*, *52*(4), 647–667. https://doi.org/10.1016/j.dsr.2004.10.010

Gula, J., Blacic, T. M., & Todd, R. E. (2019). Submesoscale coherent vortices in the Gulf Stream. *Geophysical Research Letters*, *46*(5), 2704–2714. https://doi.org/10.1029/2019GL081919

Gula, J., Theetten, S., Cambon, G., & Roullet, G. (2021). Description of the GIGATL simulations [Dataset]. *Zenodo*. https://doi.org/10.5281/zenodo.4948523

Hellweger, F. L., & Gordon, A. L. (2002). Tracing Amazon River water into the Caribbean Sea. *Journal of Marine Research*, *60*(4), 537–549. https://doi.org/10.1357/002224002762324202

Hogg, N. G., & Stommel, H. M. (1985). The Heton, an elementary interaction between discrete baroclinic geostrophic vortices, and its implications concerning eddy heat-flow. *Proceedings of the Royal Society of London. A. Mathematical and Physical Sciences*, *397*(1812), 1–20. https://doi.org/10.1098/rspa.1985.0001

Hogg, N. G., & Stommel, H. M. (1990). How currents in the upper thermocline could advect meddies deeper down. *Deep-Sea Research, Part A: Oceanographic Research Papers*, *37*(4), 613–623. https://doi.org/10.1016/0198-0149(90)90093-B

Isern-Fontanet, J., Font, J., García-Ladona, E., Emelianov, M., Millot, C., & Taupier-Letage, I. (2004). Spatial structure of anticyclonic eddies in the Algerian basin (Mediterranean Sea) analyzed using the Okubo–Weiss parameter. *Deep Sea Research Part II: Topical Studies in Oceanography*, *51*(25–26), 3009–3028. https://doi.org/10.1016/j.dsr2.2004.09.013

Jacob, J. P., Chassignet, E. P., & Dewar, W. K. (2002). Influence of topography on the propagation of isolated eddies. *Journal of Physical Oceanography*, *32*(10), 2848–2869. https://doi.org/10.1175/1520-0485(2002)032⟨2848:IOTOTP⟩2.0.CO;2

Johns, W. E., Lee, T. N., Schott, F. A., Zantopp, R. J., & Evans, R. H. (1990). The North Brazil Current retroflection: Seasonal structure and eddy variability. *Journal of Geophysical Research*, *95*(C12), 22103–22120. https://doi.org/10.1029/JC095iC12p22103

Johns, W. E., J, Z. R., & Goni, G. J. (2003). Cross-gyre transport by North Brazil Current rings. In *Elsevier oceanography series* (Vol. 68, pp. 411–441). Elsevier. https://doi.org/10.1016/S0422-9894(03)80156-3

Karstensen, J., Lavik, G., Acquistapace, C., Baghen, G., Begler, C., Bendinger, A., et al. (2020). *EUREC4A Campaign, Cruise No. MSM89, 17. January-20. February 2020, Bridgetown (Barbados)-Bridgetown (Barbados), The ocean mesoscale component in the EUREC4A++ field study*. Gutachterpanel Forschungsschiffe. https://doi.org/10.2312/cr_msm89

Käse, R. H., & Zenk, W. (1987). Reconstructed Mediterranean salt lens trajectories. *Journal of Physical Oceanography*, *17*(1), 158–163. https://doi.org/10.1175/1520-0485(1987)017<0158:rmslt>2.0.co;2

Kirchner, K., Rhein, M., Hüttl-Kabus, S., & Böning, C. W. (2009). On the spreading of South Atlantic Water into the Northern Hemisphere. *Journal of Geophysical Research*, *114*(C5), C05019. https://doi.org/10.1029/2008JC005165

Klocker, A., & Marshall, D. P. (2014). Advection of baroclinic eddies by depth mean flow. *Geophysical Research Letters*, *41*(10), 3517–3521. https://doi.org/10.1002/2014GL060001

Kolodziejczyk, N., Llovel, W., & Portela, E. (2019). Interannual variability of upper ocean water masses as inferred from Argo array. *Journal of Geophysical Research: Oceans*, *124*(8), 6067–6085. https://doi.org/10.1029/2018JC014866

Krelling, A. P., da Silveira, I. C., Polito, P. S., Gangopadhyay, A., Martins, R. P., Lima, J. A. M., & Marin, F. D. O. (2020). A newly observed quasi-stationary subsurface anticyclone of the North Brazil Undercurrent at 4S: The Potiguar Eddy. *Journal of Geophysical Research: Oceans*, *125*(10), e2020JC016268. https://doi.org/10.1029/2020JC016268

LaCasce, J. H. (1998). A geostrophic vortex over a slope. *Journal of Physical Oceanography*, *28*(12), 2362–2381. https://doi.org/10.1175/1520-0485(1998)028⟨2362:AGVOAS⟩2.0.CO;2

Lazaneo, C. Z., Calil, P. H. R., Tandon, A., & da Silveira, I. C. (2022). Submesoscale coherent vortices in the South Atlantic Ocean: A pathway for energy dissipation. *Journal of Geophysical Research: Oceans*, *127*(2), e2020JC017099. https://doi.org/10.1029/2020JC017099

Li, H., Xu, F., & Wang, G. (2022). Global mapping of mesoscale eddy vertical tilt. *Journal of Geophysical Research: Oceans*, *127*(11), e2022JC019131. https://doi.org/10.1029/2022JC019131

Marchesiello, P., Capet, X., Menkes, C., & Kennan, S. C. (2011). Submesoscale dynamics in tropical instability waves. *Ocean Modelling*, *39*(1–2), 31–46. https://doi.org/10.1016/j.ocemod.2011.04.011

Marshall, J., & Parthasarathy, B. (1993). Tearing of an aligned vortex by a current difference in two-layer quasi-geostrophic flow. *Journal of Fluid Mechanics*, *255*(-1), 157–182. https://doi.org/10.1017/S0022112093002435

Mason, E., Pascual, A., & McWilliams, J. C. (2014). A new sea surface height–based code for oceanic mesoscale eddy tracking. *Journal of Atmospheric and Oceanic Technology*, *31*(5), 1181–1188. https://doi.org/10.1175/JTECH-D-14-00019.1

McCoy, D., Bianchi, D., & Stewart, A. L. (2020). Global observations of submesoscale coherent vortices in the ocean. *Progress in Oceanography*, *189*, 102452. https://doi.org/10.1016/j.pocean.2020.102452

McWilliams, J. C. (1985). Submesoscale, coherent vortices in the ocean. *Reviews of Geophysics*, *23*(2), 165–182. Retrieved from https://agupubs.onlinelibrary.wiley.com/doi/abs/10.1029/RG023i002p00165

Metcalf, W. G., & Stalcup, M. C. (1967). Origin of the Atlantic equatorial undercurrent. *Journal of Geophysical Research*, *72*(20), 4959–4975. https://doi.org/10.1029/JZ072i020p04959

Mill, G. N., da Costa, V. S., Lima, N. D., Gabioux, M., Guerra, L. A. A., & Paiva, A. M. (2015). Northward migration of Cape São Tomé rings, Brazil. *Continental Shelf Research*, *106*, 27–37. https://doi.org/10.1016/j.csr.2015.06.010

Morel, Y., Morvan, G., Benshila, R., Renault, L., Gula, J., & Auclair, F. (2023). An "objective" definition of potential vorticity. generalized evolution equation and application to the study of coastal upwelling instability. *Ocean Modelling*, *186*, 102287. https://doi.org/10.1016/j.ocemod.2023.102287

Morrow, R., Fu, L.-L., Ardhuin, F., Benkiran, M., Chapron, B., Cosme, E., et al. (2019). Global observations of fine-scale ocean surface topography with the Surface Water and Ocean Topography (SWOT) mission. *Frontiers in Marine Science*, *6*, 232. https://doi.org/10.3389/fmars.2019.00232

Morvan, M., l'Hégaret, P., Carton, X., Gula, J., Vic, C., de Marez, C., et al. (2019). The life cycle of submesoscale eddies generated by topographic interactions. *Ocean Science*, *15*(6), 1531–1543. https://doi.org/10.5194/os-15-1531-2019

Napolitano, D. C., Carton, X., & Gula, J. (2024). NBC rings identification [Software, Dataset]. *Zenodo*. https://doi.org/10.5281/zenodo.10636521

Napolitano, D. C., Rocha, C. B., Silveira, I. C., Simoes-Sousa, I. T., & Flierl, G. R. (2021). Can the Intermediate Western Boundary Current recirculation trigger the Vitória eddy formation? *Ocean Dynamics*, *71*(3), 281–292. https://doi.org/10.1007/s10236-020-01437-6

Napolitano, D. C., Silveira, I. C., Tandon, A., & Calil, P. H. R. (2020). Submesoscale phenomena due to the Brazil Current crossing of the Vitória-Trindade Ridge. *Journal of Geophysical Research: Oceans*, *126*(1), e2020JC016731. https://doi.org/10.1029/2020JC016731

Napolitano, D. C., Silveira, I. C. A., Rocha, C. B., Flierl, G. R., Calil, P. H. R., & Martins, R. P. (2019). On the steadiness and instability of the Intermediate Western Boundary Current between 24 and 18S. *Journal of Physical Oceanography*, *49*(12), 3127–3143. https://doi.org/10.1175/JPO-D-19-0011.1

Nof, D., & Dewar, W. K. (1994). Alignment of lenses: Laboratory and numerical experiments. *Deep Sea Research Part I: Oceanographic Research Papers*, *41*(8), 1207–1229. https://doi.org/10.1016/0967-0637(94)90041-8

Nof, D., & Pichevin, T. (1996). The retroflection paradox. *Journal of Physical Oceanography*, *26*(11), 2344–2358. https://doi.org/10.1175/1520-0485(1996)026⟨2344:TRP⟩2.0.CO;2

Okubo, A. (1970). Horizontal dispersion of floatable particles in the vicinity of velocity singularities such as convergences. In *Deep sea research and oceanographic abstracts* (Vol. 17, pp. 445–454). https://doi.org/10.1016/0011-7471(70)90059-8

Pegliasco, C., Delepoulle, A., Mason, E., Morrow, R., Faugère, Y., & Dibarboure, G. (2022). META3.1exp: A new global mesoscale eddy trajectory atlas derived from altimetry. *Earth System Science Data*, *14*(3), 1087–1107. https://doi.org/10.5194/essd-14-1087-2022

Polvani, L. M. (1991). Two-layer geostrophic vortex dynamics. Part 2. Alignment and two-layer V-states. *Journal of Fluid Mechanics*, *225*, 241–270. https://doi.org/10.1017/S0022112091002045

Qu, L., Thomas, L., & Gula, J. (2021). Bottom mixing enhanced by tropical storm-generated near-inertial waves entering critical layers in the Straits of Florida. *Geophysical Research Letters*, *48*(15), e2021GL093773. https://doi.org/10.1029/2021GL093773

Reinaud, J. N., & Carton, X. (2020). The alignment of two three-dimensional quasi-geostrophic vortices. *Geophysical & Astrophysical Fluid Dynamics*, *114*(4–5), 524–560. https://doi.org/10.1080/03091929.2019.1653462

Rhein, M., Kirchner, K., Mertens, C., Steinfeldt, R., Walter, M., & Fleischmann-Wischnath, U. (2005). Transport of South Atlantic water through the passages south of Guadeloupe and across 16 N, 2000–2004. *Deep Sea Research Part I: Oceanographic Research Papers*, *52*(12), 2234–2249. https://doi.org/10.1016/j.dsr.2005.08.003

Richardson, P., Hufford, G., Limeburner, R., & Brown, W. (1994). North Brazil current retroflection eddies. *Journal of Geophysical Research*, *99*(C3), 5081–5093. https://doi.org/10.1029/93JC03486

Ruan, X., Wenegrat, J. O., & Gula, J. (2021). Slippery bottom boundary layers: The loss of energy from the general circulation by bottom drag. *Geophysical Research Letters*, *48*(19), e2021GL094434. https://doi.org/10.1029/2021GL094434

Saha, S., Moorthi, S., Pan, H.-L., Wu, X., Wang, J., Nadiga, S., et al. (2010). The NCEP climate forecast system reanalysis. *Bulletin of the American Meteorological Society*, *91*(8), 1015–1058. https://doi.org/10.1175/2010BAMS3001.1

Schmid, C., Schäfer, H., Zenk, W., & Podestá, G. (1995). The Vitória Eddy and its relation to the Brazil Current. *Journal of Physical Oceanography*, *25*(11), 2532–2546. https://doi.org/10.1175/1520-0485(1995)025⟨2532:TVEAIR⟩2.0.CO;2

Shchepetkin, A. F., & McWilliams, J. C. (2005). The regional oceanic modeling system (ROMS): A split-explicit, free-surface, topography-following-coordinate oceanic model. *Ocean Modelling*, *9*(4), 347–404. https://doi.org/10.1016/j.ocemod.2004.08.002

Silveira, I. C., Brown, W. S., & Flierl, G. R. (2000). Dynamics of the North Brazil Current retroflection region from the western tropical Atlantic experiment observations. *Journal of Geophysical Research*, *105*(C12), 28559–28583. https://doi.org/10.1029/2000JC900129

Silveira, I. C., Lima, J. A., Schmidt, A. C., Ceccopieri, W., Sartori, A., Francisco, C. P., & Fontes, R. F. (2008). Is the meander growth in the Brazil Current system off Southeast Brazil due to baroclinic instability? *Dynamics of Atmospheres and Oceans*, *45*(3–4), 187–207. https://doi.org/10.1016/j.dynatmoce.2008.01.002

Silveira, I. C., Pereira, F., Flierl, G. R., Simoes-Sousa, I. T., Palóczy, A., Borges-Silva, M., & Rocha, C. B. (2023). The Brazil Current quasi-stationary unstable meanders at 22S–23S. *Progress in Oceanography*, *210*, 102925. https://doi.org/10.1016/j.pocean.2022.102925

Simoes-Sousa, I. T., Silveira, I. C., Tandon, A., Flierl, G. R., Ribeiro, C. H., & Martins, R. P. (2021). The Barreirinhas eddies: Stable energetic anticyclones in the near-equatorial South Atlantic. *Frontiers in Marine Science*, *8*, 617011. https://doi.org/10.3389/fmars.2021.617011

Speich, S., Reverdin, G., Bellenger, H., Carton, X., Labaste, M., Noisel, C., et al. (2021). *Eurec4a-oa. cruise report. 19 January–19 February 2020*. vessel: L'Atalante. https://doi.org/10.13155/80129

Stevens, B., Bony, S., Farrell, D., Ament, F., Blyth, A., Fairall, C., et al. (2021). EUREC4A. Earth system science data discussions, 2021 (pp. 1–78). https://doi.org/10.5194/essd-13-4067-2021

Stramma, L., & Schott, F. (1999). The mean flow field of the Tropical Atlantic Ocean. *Deep Sea Research Part II: Topical Studies in Oceanography*, *46*(1–2), 279–303. https://doi.org/10.1016/S0967-0645(98)00109-X

Subirade, C., L'Hégaret, P., Speich, S., Laxenaire, R., Karstensen, J., & Carton, X. (2023). Combining an eddy detection algorithm with in-situ measurements to study North Brazil Current Rings. *Remote Sensing*, *15*(7), 1897. https://doi.org/10.3390/rs15071897

Tagliabue, A., Lough, A. J., Vic, C., Roussenov, V., Gula, J., Lohan, M. C., et al. (2022). Mechanisms driving the dispersal of hydrothermal iron from the northern Mid Atlantic Ridge. *Geophysical Research Letters*, *49*(22), e2022GL100615. https://doi.org/10.1029/2022GL100615

Tuchen, F. P., Brandt, P., Lübbecke, J. F., & Hummels, R. (2022). Transports and pathways of the tropical AMOC return flow from Argo data and shipboard velocity measurements. *Journal of Geophysical Research: Oceans*, *127*(2), e2021JC018115. https://doi.org/10.1029/2021JC018115

Tychensky, A., & Carton, X. (1998). Hydrological and dynamical characterization of meddies in the Azores region: A paradigm for baroclinic vortex dynamics. *Journal of Geophysical Research*, *103*(C11), 25061–25079. https://doi.org/10.1029/97JC03418

Umlauf, L., & Burchard, H. (2003). A generic length-scale equation for geophysical turbulence models. *Journal of Marine Research*, *61*(2), 235–265. https://doi.org/10.1357/002224003322005087

Vandermeirsch, F., Morel, Y., & Sutyrin, G. (2001). The net advective effect of a vertically sheared current on a coherent vortex. *Journal of Physical Oceanography*, *31*(8), 2210–2225. https://doi.org/10.1175/1520-0485(2001)031⟨2210:TNAEOA⟩2.0.CO;2

Vandermeirsch, F., Morel, Y., & Sutyrin, G. (2002). Resistance of a coherent vortex to a vertical shear. *Journal of Physical Oceanography*, *32*(11), 3089–3100. https://doi.org/10.1175/1520-0485(2002)032⟨3089:ROACVT⟩2.0.CO;2

Vic, C., Hascoët, S., Gula, J., Huck, T., & Maes, C. (2022). Oceanic mesoscale cyclones cluster surface Lagrangian material. *Geophysical Research Letters*, *49*(4), e2021GL097488. https://doi.org/10.1029/2021GL097488

Walsh, D., Richardson, P. L., & Lynch, J. (1996). Observations of tilting meddies. *Journal of Physical Oceanography*, *26*(6), 1023–1038. https://doi.org/10.1175/1520-0485(1996)026⟨1023:OOTM⟩2.0.CO;2

Weiss, J. (1991). The dynamics of the enstrophy transfer in two-dimensional turbulence. *Physica D*, *48*(2–3), 273–294. https://doi.org/10.1016/0167-2789(91)90088-Q

Wilson, W. D., Johns, W. E., & Garzoli, S. L. (2002). Velocity structure of North Brazil Current rings. *Geophysical Research Letters*, *29*(8), 114–121. https://doi.org/10.1029/2001GL013869

Zhang, X., Zhang, Z., McWilliams, J. C., Sun, Z., Zhao, W., & Tian, J. (2022). Submesoscale coherent vortices observed in the northeastern South China Sea. *Journal of Geophysical Research: Oceans*, *127*(2), e2021JC018117. https://doi.org/10.1029/2021JC018117

Zhang, Z., Liu, Y., Qiu, B., Luo, Y., Cai, W., Yuan, Q., et al. (2023). Submesoscale inverse energy cascade enhances Southern Ocean eddy heat transport. *Nature Communications*, *14*(1), 1335. https://doi.org/10.1038/s41467-023-36991-2

Zhang, Z., Wang, W., & Qiu, B. (2014). Oceanic mass transport by mesoscale eddies. *Science*, *345*(6194), 322–324. https://doi.org/10.1126/science.1252418